CHEMISTRY
AN ASIAN JOURNAL
www.chemasianj.org

Accepted Article

Title: Strongly Luminescent Cyclometalated Gold(III) Complexes Supported by Bidentate Ligands Displaying Intermolecular Interactions and Tunable Emission Energy

Authors: Chi-Ming Che, Kaai Tung Chan, Glenna So Ming Tong, Qingyun Wan, Gang Cheng, and Chen Yang

This manuscript has been accepted after peer review and appears as an Accepted Article online prior to editing, proofing, and formal publication of the final Version of Record (VoR). This work is currently citable by using the Digital Object Identifier (DOI) given below. The VoR will be published online in Early View as soon as possible and may be different to this Accepted Article as a result of editing. Readers should obtain the VoR from the journal website shown below when it is published to ensure accuracy of information. The authors are responsible for the content of this Accepted Article.

To be cited as: *Chem. Asian J.* 10.1002/asia.201700686

Link to VoR: http://dx.doi.org/10.1002/asia.201700686

A Journal of

ACES
Asian Chemical Editorial Society

A sister journal of **Angewandte Chemie** and **Chemistry – A European Journal**

WILEY-VCH

10.1002/asia.201700686

WILEY-VCH

Strongly Luminescent Cyclometalated Gold(III) Complexes Supported by Bidentate Ligands Displaying Intermolecular Interactions and Tunable Emission Energy

Kaai Tung Chan,[a] Glenna So Ming Tong,[a] Qingyun Wan,[a] Gang Cheng,[a][b] Chen Yang[a] and Chi-Ming Che*[a][b]

Dedication ((optional))

Abstract: A series of charge-neutral Au(III) complexes, which comprise of dicarbanionic C-deprotonated biphenyl ligand and bidentate ancillary ligands ([Au(C^C)(L^X)]; L^X = β-diketonate and relatives (O^O), quinolinolate and relatives (N^O), and diphosphino (P^P) ligands), were prepared. All the complexes are emissive in degassed CH_2Cl_2 solutions and in thin-film samples with Φ_{em} up to 18% and 35% respectively, except **5** and **6**, which bears (N^O)-type ancillary ligands. Variation of the electronic characteristics of the β-diketonate ancillary ligand was demonstrated to be a viable route for tuning the emission colour from blue-green (peak λ_{em} at ca. 466 nm for **1** and **2**; 501 nm for **4a** and **4b**) to orange (peak λ_{em} at 585 nm for **3**), in contrast to the common observations that the ancillary ligand has a negligible effect on the excited state energy of the Au(III) complexes reported in the literature. DFT/TDDFT calculations revealed that the energies of the $^3\pi\pi^*$(C^C) and the ^{3}ILCT(O^O) excited states (ILCT = intraligand charge transfer) switch in order on going from O^O = acac (acac = acetylacetonate) to aryl-substituted β-diketonate ligand. Solution-processed and vacuum-deposited OLED devices of selected complexes were prepared. The vacuum deposited OLED fabricated with **2** displays a sky blue emission with a maximum EQE of 6.71% and CIE coordinates of (0.22, 0.40). The crystal structures of **7** and **9** reveal short intermolecular Au(III)···Au(III) contacts, with intermetal distances of 3.408 and 3.453 Å, respectively. DFT/TDDFT calculations were performed on **7** and **9** to account for the non-covalent interactions. Solid samples of **1**, **3** and **9** exhibit excimeric emission at room temperature, which is rarely reported in Au(III) complexes.

Introduction

The study of gold(III) complexes for their application in medicines,[1] catalysis[2] and, more recently, organic electronics[3] is a burgeoning area. It has been widely conceived that the photoluminescent properties of Au(III) complexes are inferior to their Pt(II) counterparts. Many luminescent Au(III) complexes are only weakly emissive in solutions at room temperature. However with the persistent effort from different groups to develop new luminescent Au(III) complexes, the emission quantum yields of ~50% have recently been achieved.[3b,3c,4j] Nevertheless, the examples of Au(III) complexes with emission quantum yields >10% in solutions are still limited, examples of which are depicted in Figure 1.

Among the combination of ligands used for the construction of luminescent Au(III) complexes as depicted in Figure 2, the combination of C-deprotonated tridentate [C^N^C] ligand accompanied by an ancillary monodentate ligand is commonly adopted.[3,4] The [Au(C^N^C)(C≡CR)] complexes have been intensively studied and dominated over other Au(III) complexes to act as phosphorescent OLED dopants with reasonable to good device performance.[3] Another class of Au(III) complexes of potential interest in the development of OLED emitters is the ones supported by bidentate cyclometalated [C^N] ligands together with two ancillary monodentate ligands.[5] However, the stability of this class of complexes with the formula [Au(C^N)L_2] (where L = aryl or acetylide) is not optimistic, as reductive elimination is commonly observed when both ancillary ligands are aryl or acetylide.[5a,b] In the perspective of developing for practical applications, improving both the stability and emission quantum yields of luminescent Au(III) complexes are highly desirable. It is well-established that the stability of coordination complexes goes in the order of tetradentate> tridentate> bidentate> monodentate ligands, termed the chelate effect.[6] This also explains the fact that emitters containing unchelated monodentate ligands are seldom engaged in practical OLED application. An appealing strategy would be to design charge neutral luminescent Au(III) complexes supported by rigid trianionic tetradentate ligand systems which impart structural rigidity and at the same time, reduce non-radiative decay. However, the synthesis and structural modification of these complexes could be a formidable challenge.[3b] As a compromise we envisage that Au(III) complexes supported by two bidentate ligands, apart from being more easily prepared, would provide robustness and greater versatility to tune the electronic structures and thereby the photophysical properties. We are aware that there are only scattered examples of luminescent Au(III) complexes comprising only bidentate ligands,[7] and those displaying strong luminescence other than our previous work on [Au(C^N)(bisNHC)],[7a] are rarely found in the literature.

[a] Dr. K. T. Chan, Dr. G. S. M. Tong, Q. Wan, Dr. G. Cheng, Dr. C. Yang, Prof. Dr. C.-M. Che
State Key Laboratory of Synthetic Chemistry, Institute of Molecular Functional Materials
Department of Chemistry, The University of Hong Kong
Pokfulam Road, Hong Kong SAR (China)
E-mail: cmche@hku.hk
[b] Dr. G. Cheng, Prof. Dr. C.-M. Che
HKU Shenzhen Institute of Research and Innovation
Shenzhen, Guangdong, 518053 (China)

Supporting information for this article is given via a link at the end of the document.

For internal use, please do not delete. Submitted_Manuscript

This article is protected by copyright. All rights reserved.

Accepted Manuscript

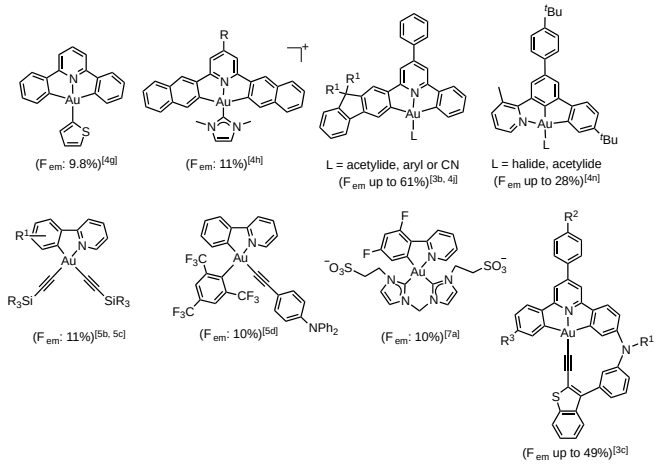

Figure 1. Selected examples of luminescent cyclometalated Au(III) complexes

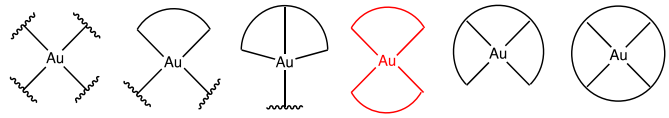

Figure 2. Possible ligands combination in Au(III) complexes.

In this work, a series of charge neutral gold(III) complexes **1–11** with the formula [Au(C^C)(L^X)] were prepared (L^X = O^O (**1–4, 7–9**), N^O (**5**,**6**), or P^P (**10,11**); Figure 3). The use of two bidentate ligands is envisaged to improve: 1) the stability of Au(III) complexes, due to the chelate effect,[6] and 2) the luminescence efficiency by imparting rigidity and thereby, restraining structural distortion in the emissive excited states relative to those with monodentate ligands.[8] Additionally, the C-deprotonated cyclometalated biphenyl ligand carrying two strong σ-donating carbon atoms is conceived to destabilize the anti-bonding Au $5d_{x^2-y^2}$ orbital, population of which would lead to facile non-radiative decay. In the literature, robust and strongly luminescent Ir(III) and Pt(II) complexes supported by bidentate ligands can be found.[9,10] Notable examples are $Ir(C^N)_2(acac)$[9a,b] and Pt(C^N)(acac)[10a] (acac = β-diketonate), both of which are thermally stable, strongly emissive, and demonstrate strong capability for fabricating into practical OLEDs with good device performances. This work represents a comprehensive demonstration of the bidentate gold(III) system, [Au(C^C)(L^X)], acting as new phosphorescent metal emitters.

We have been able to achieve strongly luminescent Au(III) complexes with tunable emission energy, particularly, sky-blue to orange emission. In addition, several interesting highlights of the system, e.g., short intermetal distances and excimeric emissions which have been well-documented in luminescent platinum(II) complexes[11] but rarely reported for gold(III) systems,[12] are reported herein.

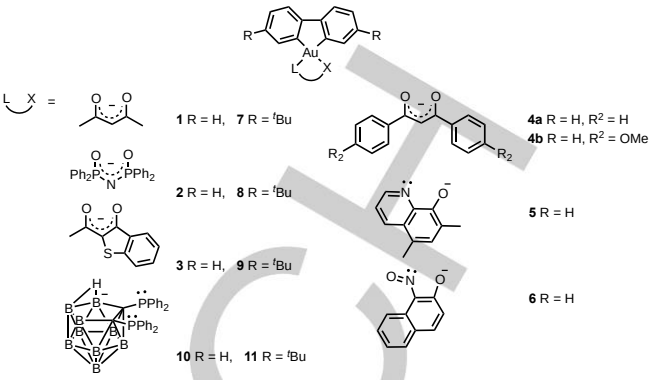

Figure 3. Au(III) complexes prepared in this work.

Results

Synthesis and characterization

In this work, transmetalation using Sn(IV) dibenzo-stannole[13] was utilized to prepare the $Au^{III}(C^C)$ precursor complexes, $[Au(C^C)Cl]_2$ and $[Au(^tBuC^C)Cl]_2$. Heating a mixture of dibenzo-stannole and $HAuCl_4{\cdot}3H_2O$ in acetonitrile at 80 °C afforded precipitates within 0.5 hr. After heating overnight, the Au(III) complexes, $[Au(C^C)Cl]_2$ and $[Au(^tBuC^C)Cl]_2$, were obtained as off-white solids in 38–50% yields (Scheme S3, Supporting Information). These precursors likely exist as dichloride-bridged dimers and are insoluble in organic solvents.[14] Dissolution only occurs upon reaction with ligands. The complexes were used in the next step of the synthesis without further purification.

Complexes **1–11** containing various ancillary bidentate ligands were obtained in 37–92% yields. Complexes **1**, **2, 4a–b, 7** and **8** were prepared by heating Na(acac) or $K(OPPh_2)_2N$ with $[Au(C^C)Cl]_2$ or $[Au(^tBuC^C)Cl]_2$ in a $CHCl_3$/EtOH mixture. The nido-carborane diphosphine complexes **10** and **11** were similarly prepared. The other complexes **3**, **5**, **6** and **9** were formed by *in-situ* deprotonation of the ligands containing a hydroxyl group in the presence of excess K_2CO_3, followed by subsequent reactions with $[Au(C^C)Cl]_2$ or $[Au(^tBuC^C)Cl]_2$ (Scheme 1). These reactions were usually complete within a few hours.

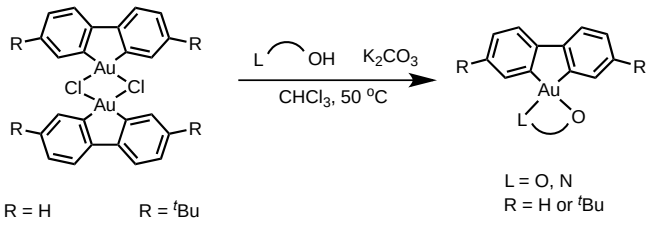

Scheme 1. Synthesis of complexes **3**, **5**, **6** and **9**.

Complexes **1–11** were characterized by ^1H, ^{13}C, ^{31}P NMR, FAB-MS and elemental analysis. The complexes are stable in the solid state and in solutions under ambient conditions. These

For internal use, please do not delete. Submitted_Manuscript

This article is protected by copyright. All rights reserved.

complexes are soluble in CH_2Cl_2 and THF but less soluble in alcoholic solvents like MeOH.

The $^{13}C_{(Au\text{-}C)}$ chemical shifts (δ) of the biphenyl ring are sensitive to *trans*-ancillary ligands: for the Au–O^O type complexes **1**–**3**, **4a**–**4b** and **7**–**9**, the $^{13}C_{(Au\text{-}C)}$ chemical shifts are at 147–151 ppm with only a small variation; for the Au–P^P type (P^P = diphosphino-nido carborane) complexes **10**–**11**, the $^{13}C_{(Au\text{-}C)}$ signal is present as a doublet of doublet and occurs at ca. 162 ppm (Figure S7, supporting information), resembling that of the recently reported Au^{III}(C^C)(P^P) (P^P = diphosphino-carborane) analog (δ = 165 ppm).[15] The $^{13}C_{(Au\text{-}C)}$ shift appears to increase with the Au–C distance determined by X-ray crystal analysis. The Au–C distances are 1.981–2.012 Å in Au–O^O type complexes (**1**–**2**, **7** and **9**) and 2.085 Å in the Au–P^P type complex (**11**). Presumably, P^P type chelating ligand exerts a stronger *trans*-effect than O^O type ones such that the Au–C bonds of the former are elongated. Consequently, the electron density of Au(III) has a less shielding effect on the $C_{(Au\text{-}C)}$ atom, leading to a more downfield $^{13}C_{(Au\text{-}C)}$ signal.

It is noteworthy that two sets of non-equivalent signals from the phenyl rings of the O^O ligand (O^O = $^{-}(OPPh_2)_2N$) are observed in the ^{13}C and ^{1}H NMR spectra of **2** and **8** respectively. Presumably, the slow flipping motion of the chelate ring renders the two neighbouring phenyl rings located at different spatial orientation in the NMR timeframe.

Thermogravimetric analysis (TGA) on **2**, **3** and **7** under nitrogen was performed. Satisfactory thermal stability with the respective onset of degradation temperature (T_d) occurring at 288, 275 and 267°C was observed (Figures S9–S11 in Supporting Information).

X-ray crystallography

Crystals of **1**, **2**, **7**, **9** and **11** were obtained by layering hexane over concentrated $CHCl_3$ solutions of complexes. For **5**, a THF/hexane mixture was used as the solvent system as decomposition was observed in concentrated chlorinated solvent. The molecular structures of **1**, **2**, **5**, **7**, **9** and **11** were determined by X-ray crystallography (Figures 4–5 and Figures S10–S11 in the supporting information) and the crystallographic data are listed in Table S3–S8, supporting information. All of the structures reveal slightly distorted planar coordination geometry. The Au–C bond distances of all except **11** lie in the range of 1.991(4)–2.024(6) Å, comparable to that of the previously reported [Au(ᵗBuC^C)(L)Cl] complexes.[14] However, in the crystal structure of [Au(C^C)(C^N)] reported by Venkatesan's group, the Au–$C_{(C^C)}$ distances are 2.030 and 2.077 Å respectively,[5a] which are slightly longer than that in **1**, **2**, **5**, **7** and **9**. This may suggest a weaker *trans*-influence imposed by the ancillary O^O or O^N compared with the C^N ligand. The C1–Au1–C12 angle ranges from 79.99(18) to 81.64(16)°, similar to that found in [Au(C^N)L_2] complexes.[5] The β-diketonate ligands in **1**, **2**, **7** and **9** form 6-membered auracycles while the O^N ligand in **5** and P^P ligand in **11** form 5-membered auracycles. Due to the steric effect imposed by the ancillary ligands, the O1**–**Au1–O2 angles of **1**, **2**, **7** and **9**, being in the range of 91.4(2)–92.55(10)°, are larger than the N1–Au1–O1 angle 79.9(2)° of **5** and P1**–**Au**–**P1' angle 80.99(4)° of **11**. Quite appealing is that *relatively short Au(III)···Au(III) contacts of 3.408 and 3.453 Å exist* in the crystal structures of **7** and **9** (Figure 6) respectively. The molecules stack in a head-to-tail fashion throughout the crystal lattice.

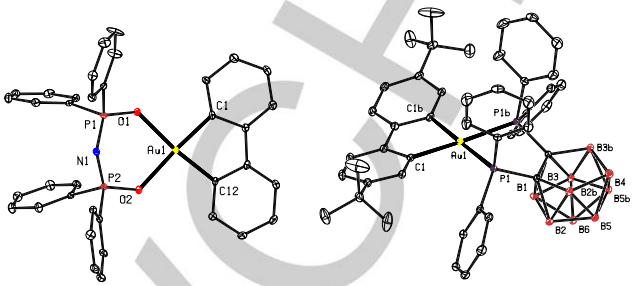

Figure 4. Perspective drawings of the crystal structures of **2** (left) and **11** (right) with the thermal ellipsoids shown at 30% probability level. Hydrogen atoms have been omitted for clarity.

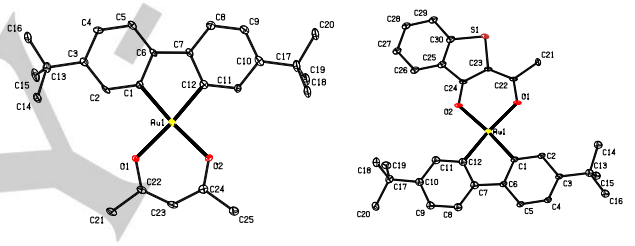

Figure 5. Perspective drawings of the crystal structures of **7** (left) and **9** (right) with the thermal ellipsoids shown at 30% probability level. Hydrogen atoms have been omitted for clarity.

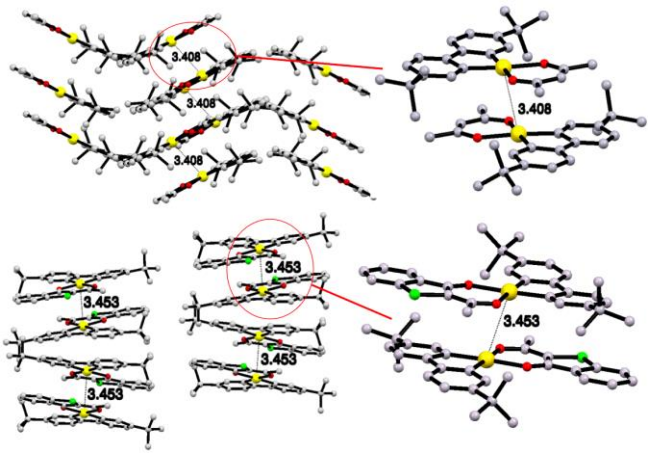

Figure 6. Perspective view of the dimeric structures of **7** (top) and **9** (bottom) revealing short Au(III)···Au(III) contacts. The interplanar distances between adjacent molecules of **7** and **9** are ca. 3.32 and 3.28 Å, respectively.

Accepted Manuscript

This article is protected by copyright. All rights reserved.

Computational study on non-covalent interactions

To account for the short intermetal distance in the dimers of **7** and **9**, the non-covalent intermolecular interactions in the dimers of **7** and **9** were examined by density functional theory (DFT) calculations at the B3LYP-D3/LANL2DZ/6-31+G* level.[16] Density functional B3LYP with the dispersion correction D3 was used due to its efficiency and accuracy in describing the dispersive interactions in non-covalent systems.[17] The solvent effect was also included using the polarizable continuum model (PCM) with dichloromethane as the solvent.

The respective optimized structures of dimers of **7** and **9** in the gas are displayed in Figure 7. The corresponding geometrical parameters of the optimized structures are depicted in Table S10 in the supporting information. The calculated Au–Au distances are 3.429 Å and 3.496 Å for **7** and **9**, respectively, in the gas phase, both of which are in good agreement with the experimental data (3.408 Å and 3.453 Å). Similar Au–Au distances were obtained when optimized in solution (see Figure S12, supporting information).

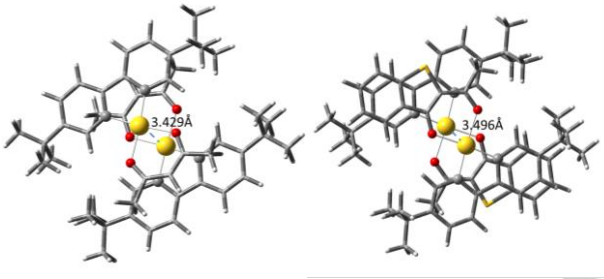

Figure 7. Optimized structures of **7** (left) and **9** (right) in the gas phase.

To gain further insight in the relatively short Au–Au distance, the total dispersion energy (E_{disp}) was decomposed into two parts: the metal-involved dispersion term (M–M and M–L) and the ligand-ligand dispersion term (L–L'). Table 1 shows that the interactions between the dimers mainly (>80%) come from the dispersion effect between the ligands (cyclometalated C^C ligand and ancillary β-diketonate ligand), while the metal-involved dispersion energy accounts only about 20% of the total dispersion energy; similar conclusions have also been drawn by Grimme on the dimer system of $[(PhNC)_4Rh]_2^{2+}$ (PhNC = phenylisonitrile).[18]

Table 1. Dispersive contributions of the ligand fragments and metal-involved fragments in **7** and **9**.

	Model	Au–Au distance (Å)	Total E_{disp} (kcal mol^{-1})	L–L' E_{disp} (kcal mol^{-1})	Metal-involved E_{disp} (kcal mol^{-1})
7	gas	3.429	–126.88	–103.39	–23.49
7	solvent	3.452	–126.22	–102.91	–23.31
9	gas	3.496	–152.45	–127.64	–24.81
9	solvent	3.504	–151.93	–127.07	–24.86

Electrochemical properties

Cyclic voltammetry were performed on complexes **1–11**. The electrochemical data are summarized in Table S11. The cyclic voltammograms of selected complexes (**4a**, **5**, **7–10**) are shown in Figure 8; others can be found in Figures S13–S14 in the supporting information. The complexes generally display one irreversible oxidation wave with E_{pa} at ca. +0.91 V to +1.44 V (quasi-reversible for **7**, **8** and **11**; extra E_{pa} for **9**) and one irreversible reduction wave with E_{pc} at –1.76 to –2.43 V (quasi-reversible for **4a** and **4b**; extra E_{pc} for **5** and **6**). Comparing the pairs [**1**,**7**], the incorporation of *t*-butyl substituents on the [C^C] ligand presumably destabilizes the HOMO and LUMO simultaneously, resulting in cathodic shifts on both E_{pc} (–2.43 to –2.22 V; ~0.2 V) and E_{pa} (+1.27 to +1.15 V; ~0.1 V). For the pair [**10**,**11**], similar cathodic shifts on E_{pc} (~0.2 V) is observed in **11**. These oxidation and reduction waves can be attributed to the ligand-centred redox process on the cyclometalated [C^C] ligand. The comparison cannot be made for [**2**,**8**] since the E_{pa} and E_{pc} are not observed for **2** and **8** respectively.

For the pair [**3**,**9**], the oxidation (E_{pa} = [+1.18, +1.16 V]) and reduction waves (E_{pc} = [–2.00, –1.96 V]) could be attributed to the redox process on the benzothiophene (bt) moiety as the presence of *t*-butyl substituents has negligible effect on the redox potentials. This is also in line with lowest-energy absorption band being derived from ^{1}ILCT localized on the bt ligand in **3** and **9** (see UV absorption spectroscopy).

For **4a** and **4b** containing β-diketonate with phenyl (**4a**) or *p*-methoxyphenyl groups (**4b**), both E_{pa} (+1.21 to +1.03 V) and E_{pc} (–1.76 to –1.90 V) show cathodic shift accordingly. The E_{pa} and E_{pc} line with the increasing electron density from **4a** to **4b** that destabilize both the HOMO and LUMO. Therefore, these oxidation and reduction waves can be attributed to the redox process on the ancillary β-diketonate ligands.

For **5** and **6** possessing N^O type ancillary ligands, an extra reduction E_{pc} is observed at much more positive potentials (–0.77 and –0.88 V respectively) than the other complexes. These reduction waves, which is not present in other complexes, are assigned to ligand-centered reduction on the redox non-innocent N^O ancillary ligands.

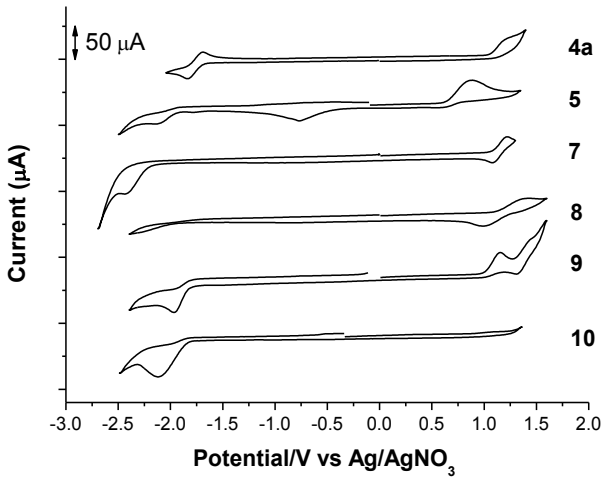

Figure 8. Cyclic voltammograms of selected complexes.

For internal use, please do not delete. Submitted_Manuscript

Accepted Manuscript

This article is protected by copyright. All rights reserved.

UV-vis absorption spectroscopy

The UV-vis absorption spectra of the gold complexes were measured in dichloromethane at room temperature. The photophysical data are summarized in Table 3 and the UV-vis absorption spectra of selected complexes are shown in Figure 9. All the complexes display intense absorption bands at λ ~ 300 nm (ε in the order of 10^4 dm^3 mol^{-1} cm^{-1}). On adding *tert*-butyl substituents to the cyclometalated biphenyl ligand as in **7**–**9** and **11**, the absorption profiles are almost identical to that of **1**–**3** and **10**, with only a subtle red shift (~3 nm) (Figure S15, supporting information). For complexes **1**, **2**, **7** and **8**, the lowest energy absorption band is at λ = 310–320 nm, with broad tails beyond ca. 350 nm and ε of ca. 1000 dm^3 mol^{-1} cm^{-1}; these absorptions could be assigned to an admixture of ^{1}IL ππ* transitions (IL = intraligand) of the cyclometalated biphenyl ligand and the ancillary ligands based on the similar absorption spectra of the respective free ligands (Figure S16, supporting information). Complexes **4a** and **4b** are derivatives of **1** containing β-diketonate ancillary ligands with methyl groups replaced by phenyl (**4a**) or *p*-methoxyphenyl (**4b**) substituents. The lowest energy absorption band of **4a** and **4b** are intense (ε ~ 2–4 × 10^4 dm^3 mol^{-1} cm^{-1}) and are red-shifted from that of **1**. This band is thus most likely derived from ^{1}IL ππ* transition localized on the β-diketonate ancillary ligands and this assignment is supported by DFT/TDDFT calculations (see supporting information). Complexes **3**, **5** and **6**, with asymmetric β-diketonate or N^O type ancillary ligands bearing low-band gap moiety of benzothiophene, quinolinolate, and nitroso-napthol, respectively, display absorption bands beyond 400 nm (Figure S18, supporting information). With reference to related works, these bands are tentatively assigned to intraligand charge transfer (^{1}ILCT) transitions of the benzothiophene β-diketonate ligand of **3** and quinolinolate ligand of **5**.[19,20] The low energy absorption in **6** is noticeably more intense (ε ~ 2 × 10^4 dm^3 mol^{-1} cm^{-1} compared to ~10^3 dm^3 mol^{-1} cm^{-1} of **3** and **5**) and is insensitive to solvent polarity and a ^{1}IL ππ* transition localized on the nitroso-napthol ligand is suggested.

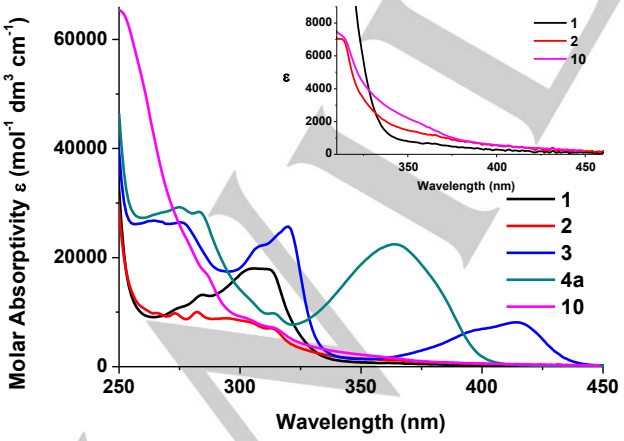

Figure 9. UV-vis absorption spectra of **1**–**3**, **4a** and **10** in CH_2Cl_2 at 298 K (2 × 10^{-5} M). Inset shows the magnified absorption tails of **1**, **2** and **10**.

Emission spectroscopy

Upon photoexcitation, all of the complexes are luminescent in degassed CH_2Cl_2 and in thin film samples at room temperature (RT), 77 K glassy solutions (EtOH/MeOH = 4:1) and in the solid state, except **5** and **6**. The emission spectra of selected complexes in CH_2Cl_2 at room temperature are depicted in Figure 10. It could be seen that upon variation of the β-diketonate ancillary ligands, the emission wavelengths could be tuned from 466 nm to 590 nm. Complexes **1**, **2**, **7** and **8** display vibronically structured blue-green emission with emission peak maxima located at 466–478 nm and vibronic-spacings of ca. 1250–1460 cm^{-1}, which agree well with the stretching frequency of C=C bonds of the biphenyl ring. Together with the large Stokes shift (~10500 cm^{-1}) between the ^{1}ππ* absorption (λ_{abs} ~ 313 nm) and emission λ_{max}, this blue-green emission is attributable to a ^{3}IL ππ* excited state localized on the cyclometalated C^C ligand. The emission spectra of **1**, **2**, **7** and **8** in glassy solutions display a 5–10 nm rigidochromic shift with respect to that in RT degassed solutions. Complexes **3** and **9**, on the other hand, display a structureless and bathochromically shifted orange emission at 585 nm, which could be assigned to a ^{3}ILCT (ILCT = intraligand charge transfer) excited state localized on the benzothiophene β-diketonate (bt) ligand, based on DFT/TDDFT calculations (*vide infra*). In 77 K glassy solutions, the emission spectra become structured and display a ~40 nm (~1100 cm^{-1}) blue shift. Except **8**, all these complexes are strongly luminescent (Φ_{em} ≈ 11–18%), with emission lifetimes in the range of 50–75 μs. Regarding the decent Φ_{em} in solution, the emission of **1**–**3**, **7**–**9** in thin-films (5 wt% PMMA or PYD-2Cz) were studied. The emission spectra resemble that obtained in degassed solution, with the highest Φ_{em} obtained from each sample being 10–35%.

Complexes **4a** and **4b**, which bear diaryl β-diketonates, display structureless emissions at lower energies (λ_{max} ~ 500 nm; (Figure S27, supporting information) with shorter emission lifetimes (τ = 2–5 μs) when compared with its analogue, **1**. This band could be assigned as ^{3}ILCT localized on the β-diketonate ancillary ligands (see computational study). The 77 K glassy solutions of **4a** and **4b** both display the vibronically-structured and long-lived emissions (λ_{em} at ca. 472, 502, 537; τ >250 μs) characteristic of ^{3}IL excited states (Figures S28–S29, supporting information).

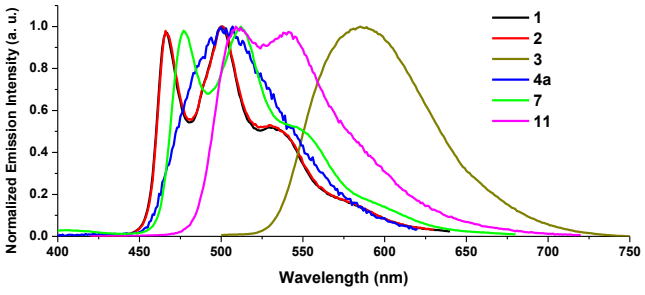

Figure 10. Emission spectra of **1**–**3**, **4a**, **7** and **11** in degassed CH_2Cl_2 at 298 K (2 × 10^{-5} M).

For internal use, please do not delete. Submitted_Manuscript

This article is protected by copyright. All rights reserved.

Table 3. Photophysical data of complexes **1–11**.

	UV-vis absorption[a]	Emission[a]				
	λ_{abs} [nm] ($10^3\varepsilon$ [$mol^{-1}dm^3\,cm^{-1}$])	Solution λ_{max} [nm] (τ [μs]; Φ_{em}[b]; k_q [10^7 mol dm^{-3} s^{-1}]; k_r; k_{nr} [10^3 s^{-1}])	Glassy 77 K (τ [μs])	Solid (τ [μs]; Φ_{solid}[e])	Solid 77 K (τ [μs])	Thin film[f] (Φ_{film}[e])
1	274 (10.7), 285 (13.2), 306 (18.0), 311 (17.9), 350 (br, 0.8)	466, 500, 534 (51; 0.11[b]; 4.1; 2.16; 17.5)	461, 496, 525 (123.9)	464, 498 (6.2; 0.09), 574(max) (455)	465, 501, 533 (74.0)	467, 503, 535 (0.15)
2	266 (9.8), 273 (9.8), 282 (10.0), 294 (8.9), 313 (7.0), 350 (br, 1.4)	467, 501, 533 (53; 0.14[b]; 0.7; 2.64; 16.2)	461, 496, 525 (121.6)	466, 501, 532 (101.6; 0.48)	463, 499, 540 (112.3)	467, 502, 535 (0.35)
3	264 (26.8), 275 (26.5), 308 (22.1), 320 (25.7), 398 (6.8), 414 (8.1)	585 (174.5; 0.16[c]; 1.3; 0.92; 4.81)	550, 584 (795)	552 (9.8; 0.13), 592 (9.7), 659, 674 (539)	583 (509.6)	564 (0.02, 0.07[h]); 570 (0.23[g], 0.33[h])
4a	275 (29.2), 283 (28.4), 315 (9.6), 363 (22.4)	502 (2.1; 0.006[b]; 0.97; 2.86; 473)	472, 502, 537 (249.4)	441(fl), 489, 518, 563 (2.1)	512, 543, 589(sh) (107.3)	–
4b	293 (34.6), 375 (37.6)	501 (5.5; 0.02[b]; 1.1; 4.36; 177)	475, 505, 540 (482.0)	449, 486, 519, 571, 621 (0.2)	514 (119.2)	–
5	279 (50.7), 315 (10.7), 333 (5.1), 347 (3.9), 447 (5.8)	Non-emissive	520 (<0.1)		Non-emissive	
6	294 (39.1), 414 (20.6), 487 (5.1)	Non-emissive	440, 471, 508, 588 (16.7)		Non-emissive	
7	284 (9.9), 306 (15.5), 313 (15.7), 378 (br, 1.2)	478, 512, 547 (74.2; 0.13[b]; 0.88; 1.82; 12.2)	468, 505, 543 (159.5)	467, 501, 537 (12.3; 0.10)	484, 518, 545 (64.2)	475, 508, 548 (0.10)
8	273 (7.8), 284 (8.0), 303 (10.8), 316 (10.3), 350 (br, 1.4)	478, 512, 546 (4.9; 0.01[b]; n.d.[d]; 2.05; 203)	469, 505, 539 (166.8)	479, 514, 550 (69.5; 0.36)	474, 512, 546 (95.7)	477, 511, 547 (0.34); 478, 513, 550 (0.29[g])
9	277 (23.2), 309 (23.2), 319 (26.6), 396 (5.7), 414 (6.9)	590 (199.4; 0.18[c]; 0.34; 0.90; 4.11)	549, 586 (859)	563 (14.6; 0.09), 683	594 (268.2)	580 (0.03, 0.21[h]); 571 (0.26[g,h])
10	249 (65.4), 315 (7.0), 362 (br, 1.6)	495, 521 (0.2; 0.003[b]; n.d.[d]; 16.7; 5540)	481, 517, 553 (122.8)	492, 526 (20.3; 0.09)	498, 532, 568 (58.5)	489, 522, 560 (0.15)
11	257 (61.5), 306 (9.0), 318 (8.1), 375 (br, 1.4)	512, 541 (2.3; 0.01[b]; n.d.[d]; 4.31; 427)	496, 533, 569 (99.2)	504, 539 (41.7; 0.31)	496, 536, 577 (59.3)	506, 542 (0.18)

[a] Measurements were performed in solutions (2×10^{-5} M) at 298 K unless specified. Glassy measurements were performed in EtOH/MeOH (4:1) at 77 K. Self-quenching rate constants, radiative and non-radiative decay rate constants are denoted by k_q, k_r and k_{nr}, respectively. [b] Solution emission quantum yield (Φ_{em}) were measured using 9,10-bis(phenylethynyl)anthracene (BPEA) in benzene (Φ_{em} = 0.85) or [c] $[Ru(bpy)_3][PF_6]_2$ in degassed acetonitrile as the standard (Φ_{em} = 0.062). [d] Values were not determined (n.d.) due low Φ_{em}. [e] Absolute emission quantum yields of amorphous solid samples and thin-film samples were measured with a Hamamatsu Quantaurus-QY Absolute PL quantum yields spectrometer. [f] Thin-film emission measured in 5 wt% PMMA film unless specified. [g] Thin-film emission measured in 5 wt% PYD-2Cz film. [h] Thin-film emission data obtained when measured under N_2.

Complexes **5** and **6** bearing N^O-type ligands are non-emissive in solutions or solid states. The emission intensities remain weak even at 77 K glassy solutions. The lowest energy triplet excited states of **5** and **6** are conceived to be localized on the N^O ligands, which are likely associated with significant non-radiative decay. It is noted that the related Pt^{II}-quinolinolate complexes emit in the deep-red region with Φ_{em} <1%.[20b] Sterically-bulky nido-carborane moiety, which has been found to exhibit interesting photoluminescent properties,[21] has been incorporated into complexes **10** and **11**. Although they were weakly emissive in degassed CH_2Cl_2 solutions (Φ_{em} <1% and τ <3 μs), presumably due to the fast non-radiative decay rate (k_{nr} > 10^5 s^{-1}), they were found to be strongly emissive in the solid state and in 77 K glassy solutions. Thin-films samples of **10** and **11** (5 wt% in PMMA) exhibit Φ_{em} of 15% and 18%, respectively. In degassed CH_2Cl_2 solutions, the emission λ_{max} of **10** and **11** bathochromically shift ca. 30 nm ($\Delta\nu$ ~1300 cm^{-1}) from that of **1** and **7**. The vibronically-structured emission bands of **10** and **11** are similarly attributable to a ^{3}IL ππ* excited state localized on the [C^C] ligand. With reference to the x-ray crystal structure of **11,** the P^P ligand appears to be a stronger σ-donor than the β-diketonate ligand. The red shift of ^{3}IL(C^C) emission is presumably a result of the greater destabilization of the Au-perturbed HOMO by the P^P ligand.

For internal use, please do not delete. Submitted_Manuscript

This article is protected by copyright. All rights reserved.

Excimeric emission in the solid state

The solid-state emission spectra are recorded for all complexes (except **5** and **6**) at 298 K and 77 K. Interestingly, for complexes **1**, **3** and **9** at 298 K, apart from the high-energy emission bands which resemble the respective emission spectra measured in degassed solutions, low-energy structureless emission bands with peak λ_{em} at 574 nm, 659 nm and 683 nm are respectively observed (Figure 11a for complex **1**; Figures S24 and S33, supporting information, for complex **3** and **9**, respectively). When the same samples were cooled to 77 K, only high-energy emission bands (peak λ_{em} at 465 nm, 583 nm and 594 nm, respectively, for **1**, **3** and **9**) with emission profiles resembling those recorded in degassed CH_2Cl_2 solutions at 298 K were observed. The low-energy emission bands observed with solid samples of **1**, **3** and **9** at 298 K are tentatively assigned to excimeric emissions and the high-energy emission bands are attributable to monomeric emissions.

The excimeric emission is noticeably more intense for **3** than **9** (graph in red; Figures S24 vs S33 in the supporting information), probably due to the absence of bulky *tert*-butyl substituent on the cyclometalated C^C ligand which allows closer contact between the excited state and ground state in **3**. Attempts to observe the excimeric emission from **3** in CH_2Cl_2 solution with concentration up to 3×10^{-3} M were not successful. Higher concentrations are not possible due to the limited solubility of **3** in CH_2Cl_2.

Time-resolved emission spectroscopy was utilized to observe the decay kinetics of the solid-state emission of **1**. Emission measurements were performed with a solid sample of **1** at 298 K at different gated time intervals. The followings were observed: 1) from 0–15 μs, there was an initial decay of the vibronically-structured monomeric emission having peak maxima at 464, 498 and 534 nm (Figure 11b); 2) from 20 to 80 μs, an excimeric emission with peak λ_{em} at 574 nm emerged, along with the decay of the monomeric emission (Figure 11c); 3) from 100–1200 μs, the decay of emission entirely came from the excimer (Figure 11d). Kinetic analysis of the decay traces of the excimeric emissions of **1** and **3** gave the decay lifetimes, respectively, as 455 and 539 μs, more than 50-fold longer than their corresponding monomer emission lifetimes.

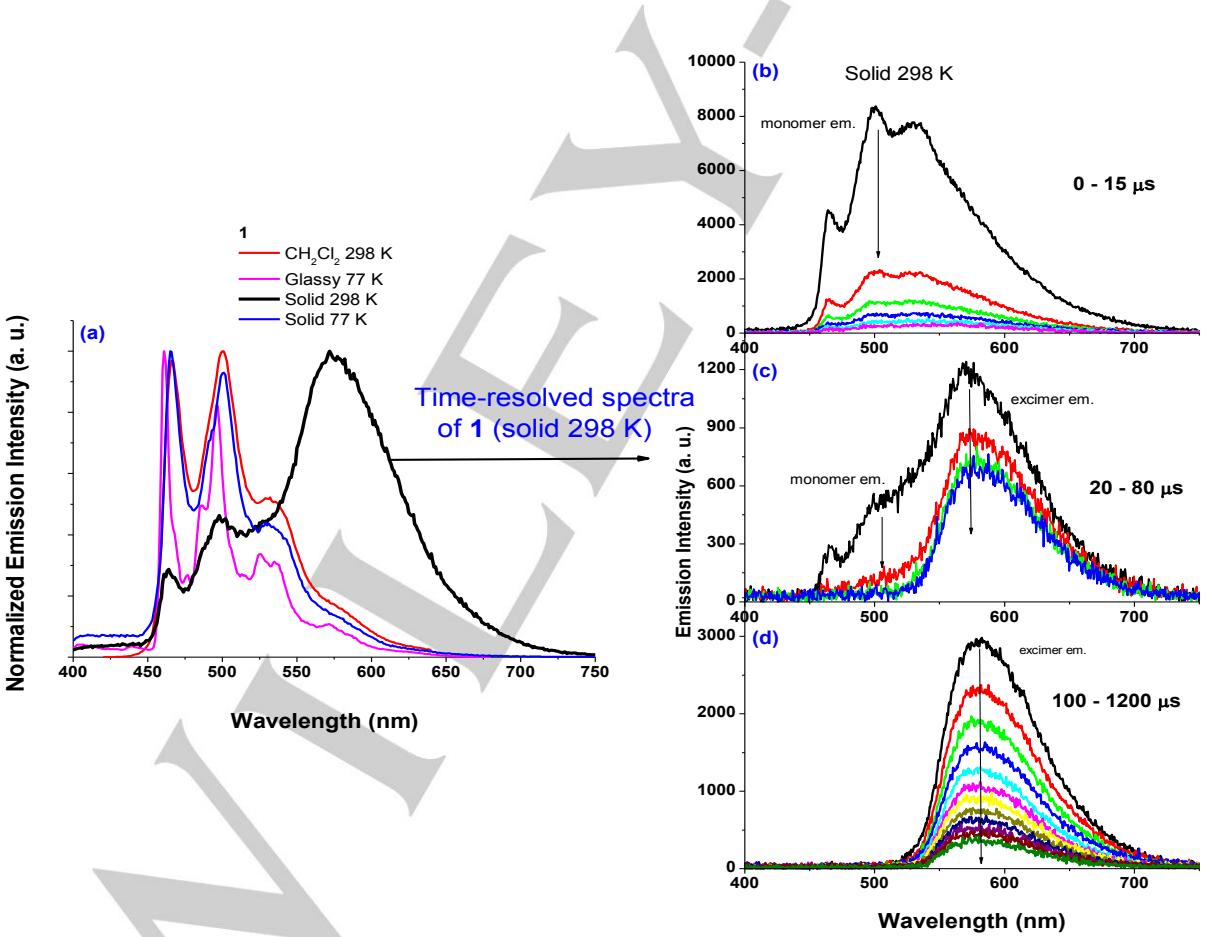

Figure 11. (a) Emission spectra of **1** in degassed CH_2Cl_2 (2×10^{-5} M), 77 K glassy solution (EtOH/MeOH = 4:1) and in the solid state at 298 K and 77 K, respectively. Time-resolved emission spectra of a solid sample of **1** at 298 K from (b) 0–15 μs, (c) 20–80 μs and (d) 100–1200 μs, with integration time of 3, 20 and 100 μs respectively. Arrows indicate the direction of spectral evolution.

For internal use, please do not delete. Submitted_Manuscript

This article is protected by copyright. All rights reserved.

Time-resolved absorption spectroscopy

Nanosecond transient absorption (ns-TA) difference spectra of **1**, **3** and **11** were recorded (Figure S40 in the supporting information and Figure 12a). These spectra are featured by positive excited state absorption (ESA) bands in the spectral range of 300–700 nm, with decay time constants of: 39.0 (**1**), 86.4, 29.0 (**3**) and 2.2 μs (**11**). The τ_{ESA} values in the microsecond timescale are attributable to the absorption of the lowest triplet excited state (T_1), i.e. $T_1 \rightarrow T_n$ absorption. The T_1 of **1** absorbs at 378 nm; it does not show any significant absorption at λ ≥ 420 nm (Figure S40, supporting information). The ns-TA spectrum of **3** is dominated by a broad ESA peaking at 504 nm (Figure 12b and a relatively less intense absorption with λ_{max} = 344 nm (Figure S40, supporting information). The distinguishing feature between the ns-TA spectra of **1** and **3** agrees with the previous assignment that their lowest triplet excited states T_1 are localized on different luminophores; ^{3}IL[C^C] for **1** and ^{3}ILCT[bt] for **3**. The ns-TA spectrum of **11** (λ_{max} = 364 nm) is similar to that of **1** except there is an extra broad band at ca. 450 nm for **11** (Figure S40, supporting information).

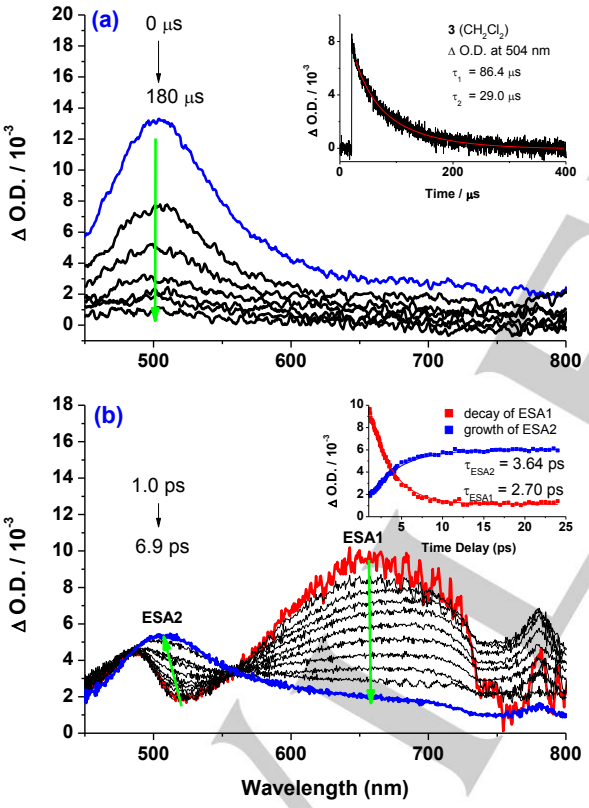

Figure 12. (a) ns-TA difference spectra (λ_{ex}: 355 nm) and (b) fs-TA difference spectra (λ_{ex}: 400 nm) and of **3** in CH_2Cl_2 (5×10^{-5} M) recorded at selected decay time at 298 K (Only showing the spectral range from 450–800 nm). The green arrows indicate the direction of spectral evolution. Insets show the kinetic time profiles and the decay time constants at the specified wavelengths. Decay lifetimes of the ns-TA and fs-TA were fitted as bi-exponential and mono-exponential decay respectively.

To further probe the early excited state dynamics, the femtosecond transient absorption (fs-TA) difference spectra of **3** at 1.0 ps to 6.9 ps (Figure 12a) were recorded. The initially formed (<1 ps) excited state absorption peaking at 657 nm (ESA1) was found to decay with a concomitant development of an excited state absorption peaking at 504 nm (ESA2), which fully developed within 1 ps and persisted up to 2600 ps. The clear isosbestic point at ~560 nm is supportive of a transformation between ESA1 and ESA2. Analyzing the kinetic profiles gave similar time constants of the decay of ESA1 (τ_{ESA1}) and growth of ESA2 (τ_{ESA2}): 2.70 ps vs 3.64 ps. In addition, comparing ESA2 at 504 nm with the ns-TA spectrum of **3** (Figure 12b), the two spectra are similar, suggesting ESA2 is attributable to the $T_1 \rightarrow T_n$ absorption. With the precursor-successor relationship between ESA1 ($S_1 \rightarrow S_n$ absorption) and ESA2 ($T_1 \rightarrow T_n$ absorption), τ_{ESA1} can be taken as the intersystem crossing time constant (τ_{ISC}), i.e., $\tau_{ISC} \approx 2.70$ ps for **3**.

Theoretical calculations on the photophysical properties

Upon variations of the β-diketonate ancillary ligand, it is possible to tune the emission colour from sky blue to orange (see Figure 10). To gain insight on the nature of the emissive excited state of these heteroleptic bidentate gold(III) complexes, DFT/TDDFT calculations were performed on complexes **1**, **4a**, and **3** (λ_{em} = 466, 502, and 585 nm respectively). At the optimized ground state geometry, the lowest intense absorption peak (λ_{calc} = 296 nm; *f* = 0.1373) for **1** corresponds to HOMO → L+1 transition and is assigned to be the $^1\pi\pi^*$(C^C) transition, whereas the first intense absorption peak for **4a** (λ_{calc} = 331 nm; *f* = 0.4767) is mainly derived from H–1 → LUMO transition and **3** (λ_{calc} = 369 nm; *f* = 0.0955) HOMO → LUMO transition, both of which could be assigned as ^{1}ILCT localized dominantly on the β-diketonate (O^O) ligand (see supporting information for the TDDFT results and Figure 13 for the relevant MO surfaces). In addition, ^{1}ILCT(O^O) of **1** is ~3000 cm^{-1} *above* the $^1\pi\pi^*$(C^C) excited state, but that of **4a** and **3** are ~3400 and 6700 cm^{-1} *below* the $^1\pi\pi^*$(C^C) excited state at the optimized S_0 geometries. This could be rationalized from the MO diagrams depicted in Figure 13. For **1** with acetylacetonate (acac) as the ancillary ligand, the HOMO is derived predominantly from π(C^C) with the H–1, being derived from a mixture of π(O^O)/Au(d)/π(C^C), lying ~0.57 eV below the HOMO; the LUMO and L+1 are respectively derived from metal-perturbed π*(O^O) and π*(C^C) with the LUMO/L+1 energy gap of only ~0.28 eV (leftmost in Figure 13). Replacing the methyl groups with phenyl groups to give **4a**, these frontier orbitals (H–1, HOMO, LUMO, and L+1) are of similar nature as **1**, but H–1 is now destabilized and is only ~0.43 eV below the HOMO; besides, the LUMO is now significantly stabilized due to extended π-conjugation with the phenyl groups and the LUMO/L+1 gap is more than 1 eV (middle in Figure 13). For **3** with the bt-substituted β-diketonate ancillary ligand, the HOMO is now localized on π(O^O) with some Au(d) character and the H–1 is localized on π(C^C); the LUMO and L+1 are also derived from π*(O^O) and π*(C^C) respectively. As the bt moiety is more electron-rich than the methyl group, the LUMO is also stabilized with respect to that of **1**, and the LUMO/L+1 gap is more than 0.8 eV (rightmost in Figure 13). As

For internal use, please do not delete. Submitted_Manuscript

This article is protected by copyright. All rights reserved.

such, the orbital energy difference relating to ππ*(C^C) would be 5.07, 5.15, and 5.06 eV for complexes **1**, **4a**, and **3** respectively, while the orbital energy difference relating to ππ*(O^O) would be 5.36, 4.51, and 4.06 eV for complexes **1**, **4a**, and **3** respectively. Thus, changing the electronic characteristics of the ancillary ligand results in a change of the relative energies of the ^{1}ππ*(C^C) and ^{1}ILCT(O^O) excited states and the first intense absorption peak red shifts going from **1** to **4a** to **3** (see Figure 9).

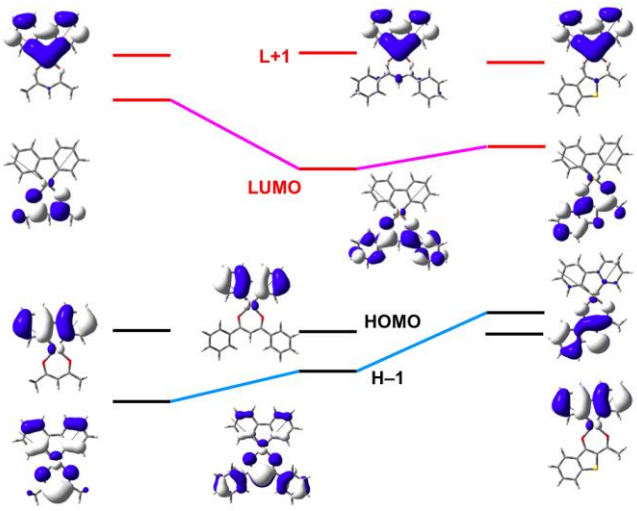

Figure 13. MO diagrams of the complexes **1** (left)**, 4a** (middle), and **3** (right) at their respective optimized S_0 geometries.

^{3}ππ*(C^C) and ^{3}ILCT(O^O) excited states have also been optimized for complexes **1**, **4a**, and **3**. Similar relative order of the ^{3}ππ*(C^C) and ^{3}ILCT(O^O) was found for these three complexes as the singlet counterparts: ^{3}ILCT(O^O) excited state is ~1600 cm^{-1} *above* the ^{3}ππ*(C^C) excited state for complex **1**, whereas that of complex **4a** and **3** are respectively 2100 and 3600 cm^{-1} *below* the ^{3}ππ*(C^C) excited state (Table S15, supporting information). Thus, the emissive triplet excited state for **1** is derived from ^{3}ππ*(C^C) while the phosphorescent excited state for **4a** and **3** both comes from the ^{3}ILCT(O^O) excited state. The calculated emission peak maxima for complexes **1**, **4a**, and **3** are 469, 512, and 586 nm respectively, in good agreements with the experimental λ_{max} (Table 2).

Aggregation and self-assembled properties

The findings of short Au(III)···Au(III) intermolecular distances in the crystal structures of **7** and **9** (Figure 3) and excimeric emissions for **1**, **3** and **9** in the solid state (Figure 11; Figure S24 and S33, supporting information) prompted us to examine the possible aggregation behaviour of these Au(III) complexes in solution and the formation of nano-/micro-structures by self-assembly.

Complexes showing aggregation in solution is often manifested by temperature and/or concentration dependence in UV-vis absorption spectra or ^{1}H NMR spectra. Variable temperature ^{1}H NMR experiments were performed with a concentrated $CDCl_3$ solution (conc.: 1.6 × 10^{-2} M, Figure S41 in the supporting information) of **7**. This complex shows a multiplet at 7.21–7.26 ppm and a singlet at ca. 7.7 ppm. Upon lowering the temperature from 25 °C to –50 °C, the chemical shift of the singlet shows a negligible change; the multiplet signals show only a mere 0.05 ppm downfield shift. The peaks become more resolved at the same time, indicating negligible aggregation in $CDCl_3$ solution even at such a high concentration of 1.6 × 10^{-2} M and low temperature. Concentration-dependent ^{1}H NMR experiments were performed on $CDCl_3$ solution of **1** and **3** (conc.: 2 × 10^{-3} to 6 × 10^{-3} M), **7** and **9** (conc.: 5 × 10^{-3} to 1.2 × 10^{-2} M). All of them show negligible shift (<0.01 ppm), concurring with negligible aggregation in solutions (Figures S42–S43 in the supporting information)

The intermolecular aggregation of **9** in CH_2Cl_2 solution was examined by UV-vis absorption spectroscopy. Increasing the concentration from 2 × 10^{-5} M to 1.6 × 10^{-2} M did not lead to obvious spectral changes apart from the increase in absorption intensity, suggesting that there are insignificant amount of **9** undergoing aggregation in this solvent. Complexes **1** and **3**, without bulky substituents on the [C^C] ligand, were not chosen for similar experiments due to their limited solubility in organic solvents; the highest concentration attained was ca. 3 × 10^{-3} M. Besides, increasing the concentration of **1** and **7** in CH_2Cl_2 from 10^{-4} to 10^{-3} M did not lead to the formation of low-energy absorption bands (Figure S19, supporting information). The effect of temperature on the UV-vis absorption spectra of **1** in CH_2Cl_2 (5 × 10^{-4} M) solution was also investigated. No spectral change was observed when the temperature was lowered from 25 °C to –50 °C except that precipitation of **1** from the solution occurred after –55 °C (Figure S20, supporting information).

The morphologies of the micro/nano-structures of **1** or **3** formed from the dispersion of hexane/dichloromethane (10:1) mixtures (2 × 10^{-4} M) of the respective complexes were examined by transmission electron microscopy (TEM). The TEM image (Figure 14a) of **1** revealed micro-rods with widths of ca. 0.1–0.2 μm and lengths of ca. 1 μm. In the case of **3**, the TEM image (Figure 14d) revealed nano-wires with diameters of ca. 0.02–0.05 μm and lengths of up to 1 micron. The selected area electron diffraction (SAED) pattern (Figure 14c) of a micro-rod of **1** revealed diffraction spots with d-spacings of 7.3 and 20.4 Å for **1**, which are in good agreement with the unit cell dimension (*b*: 7.3623(9) Å; *c*:19.871(2) Å, Table S1 in the supporting information). For the SAED pattern (Figure 14f) of a nano-wire of **3**, the d-spacings were found to be 3.6 and 12.1 Å respectively.

Accepted Manuscript

This article is protected by copyright. All rights reserved.

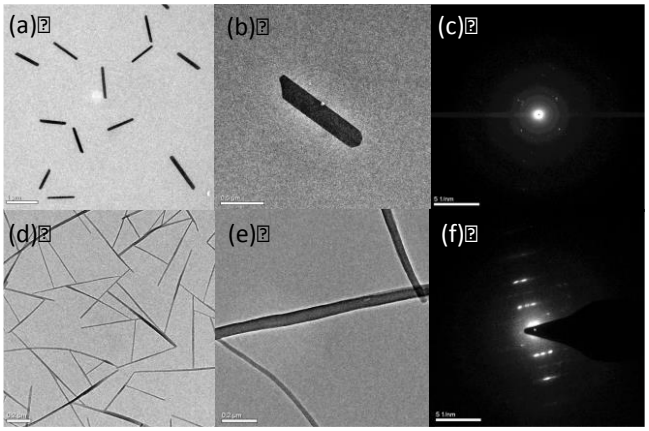

Figure 14. (a)(d) TEM images of micro-/nano-structures obtained from the dispersion of **1** and **3** in a hexane/CH_2Cl_2 mixture, respectively; (b)(e) an individual micro-rod/nano-wire and (c)(f) the corresponding SAED pattern.

Table 4. Key performance parameters of OLEDs with **2**, **8** and **9**

Complex	V_{on}[c] (V)	Max. CE (cd A^{-1})	Max. PE (lm W^{-1})	Max. EQE (%)	CIE[d] (x, y)
2[a] (10 wt%)	7.1	9.07	3.71	3.12	(0.28, 0.50)
8[a] (10 wt%)	10.5	8.88	2.44	2.94	(0.31, 0.53)
9[a] (10 wt%)	6.1	11.77	5.60	4.45	(0.54, 0.45)
2[b] (10 wt%)	2.7	17.50	20.00	6.71	(0.22, 0.40)

[a] OLED fabricated by solution process. [b] OLED fabricated by vacuum deposition. [c] Turn-on voltage (luminance = 1 cd m^{-2}). [d] CIE coordinates at 100 cd m^{-2}.

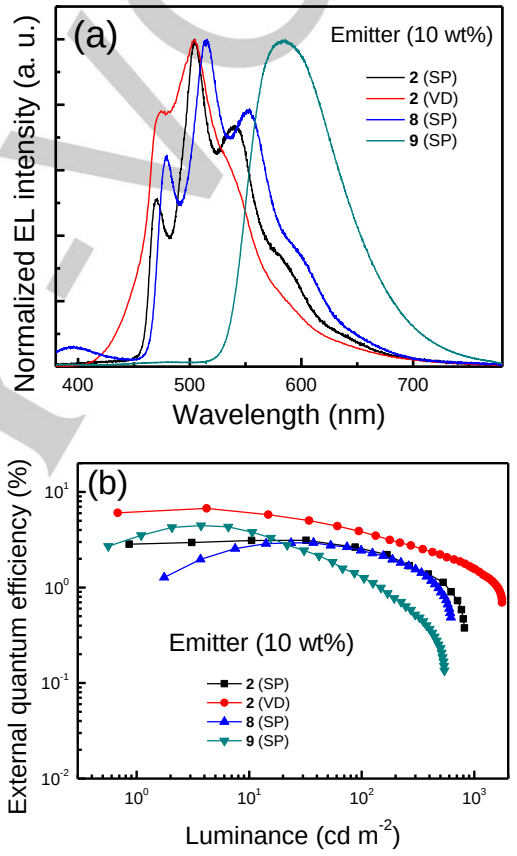

Figure 15. (a) Normalized EL spectra and (b) EQE-luminance characteristics of solution- processed (SP) OLEDs with 10 wt% **2**, **8** and **9** as well as a vacuum-deposited (VD) OLED with **2**.

Electroluminescence properties

Since the Au(III) complexes described in this work are highly emissive in solutions and in thin-film samples with PL quantum yields up to 18% and 35%, respectively, their performance as phosphorescent OLEDs dopant was examined. Complexes **2**, **8**, and **9** were chosen for investigations since they have the highest quantum yield in the film state among all the complexes studied in this work.

OLED devices based on **2**, **8** and **9** were fabricated and their electroluminescent (EL) properties were investigated. The OLEDs were solution-processed with an architecture of ITO / PEDOT:PSS / PYD2:Au(III)-emitter (40 nm) / DEPEO (5 nm) / TPBi (40 nm) / LiF (1.2 nm) / Al (Al). In these devices, 10 wt% **2**, **8** or **9** was used as the emitter.

Considering the high triplet energy ($E_t \approx 2.7$ eV) of **2** and **8**, host and charge-transporting materials having E_t >2.7 eV are needed to effectively confine the triplet excitons within the emitting layer (EML) and to block back-energy transfer to the host and/or charge transporting material(s).[22] Therefore, 2,6-dicarbazolo-1,5-pyridine (PYD2, E_t = 2.93 eV)[23a] and bis{2-[di(phenyl)phosphino]-phenyl}ether oxide (DEPEO, E_t = 3.00 eV)[23b] were used as the respective host and electron-transporting materials in the solution-processed OLEDs.

As depicted in Figure 15a, the EL emission peak maxima for the solution-processed OLEDs with **2**, **8** and **9** are identical to the corresponding PL emission peak maxima of these complexes in thin film (Table 2), suggesting efficient confinement of triplet excitons in the EML for all devices. Maximum external quantum efficiencies (EQEs) of 3.12%, 2.94%, and 4.45% were achieved for the devices fabricated with **2**, **8**, and **9**, respectively (Figure 15b). The detailed device performance data are summarized in Table 3.

To further improve the EQE of the device fabricated with **2**, a vacuum-deposited OLED with a structure of ITO/HAT-CN (5 nm) / TAPC (40 nm) / TCTA (10 nm) / POAPF: **2** (10 wt%, 20 nm) / TmPyPb (40 nm) / LiF (1.2 nm) / Al (150 nm) was fabricated and characterized. Based on the same design strategy as the solution-processed OLEDs, a high E_t material 2,7-bis(diphenylphosphoryl)-9-[4-(N,N-diphenylamino)phenyl]-9-phenylfluorene (POAPF, E_t = 2.75 eV)[23c] was used as the host. In addition, di-[4-(*N*,*N*-ditolyl-amino)-phenyl]cyclohexane (TAPC) was used as the hole-transporting layer (HTL), 4,4′,4″-tris(carbazole-9-yl)triphenylamine (TCTA) as an electron/exciton

For internal use, please do not delete. Submitted_Manuscript

This article is protected by copyright. All rights reserved.

blocking layer layer and 1,3,5-tri[(3-pyridyl)-phen-3-yl]benzene (TmPyPb) as the ETL. An improved maximum EQE of 6.71% corresponding to a current efficiency of 17.50 cd A^{-1} was achieved for the vacuum-deposited OLED with **2** (Figure 15b and Table 4). Although the EL efficiencies of the **2**-, **8**- and **9**-devices are not as high as those of the best reported data of Au(III)-OLEDs in the literature,[3b–e] the **2**-device displayed the highest EL energy (sky blue) with decent efficiency among the reported Au(III)-OLEDs in the literature (See Table S25, supporting information).

Discussion

Synthesis of the Au^{III}(C^C) complexes

In the literature, metal complexes containing the doubly deprotonated biphenyl ligand (C^C) are mostly accessed by oxidative addition of biphenylene to a low valent metal ions, or by a transmetalation method, usually by reacting the metal precursors with 2,2'-dilithiumbiphenyl.[24] For the related Au^{III}(C^C) complexes, there are only a handful of reports towards their synthesis.[5a,15,25] In this work, transmetalation using organostannyl compounds has been utilized to prepare the Au^{III}(C^C) complexes. This method was reported by Usón and co-workers three decades ago.[14] Recently, Mohr's group revisited Usón's method and successfully synthesized a series of [Au^{III}(^{t}BuC^C)] complexes.[13] This method is a better alternative towards Au^{III}(C^C) complex than the method using dilithiated biphenyl, which was usually accompanied by the reduction of gold(III) ion to elemental gold, resulting in rather low product yield.[5a]

We attempted to prepare other [Au^{III}(C^C)] complexes with modified cyclometalated [C^C] ligands (see Scheme 2); however, fast decomposition into metallic gold was observed upon stirring the organostannyl compounds with $HAuCl_4 \cdot 3H_2O$ under room temperature. Presumably, the high electron density conferred by the amino-, alkyl- and alkoxyl- substituents in these [C^C] moieties facilitated the reduction of Au(III) ion to give metallic gold.

The TGA thermal degradation curves for **2**, **3** and **7** show smooth linear slopes (Figure S9, supporting information), which signify clean degradation upon heating. There is a negligible initial weight loss until the T_d at ~280 °C is reached. Many reported bidentate Au(III) complexes easily undergo decomposition *via* reductive elimination to form homocoupled butadiynes or biaryl species.[5a,b] Incorporation of an electron-withdrawing fluorine atom or fluorine-containing substituent was suggested to be a possible means to improve the complex stability.[5a,d,f] This present work also demonstrates that bidentate β-diketonate type ancillary ligands can stabilize [Au^{III}(C^C)] complexes.

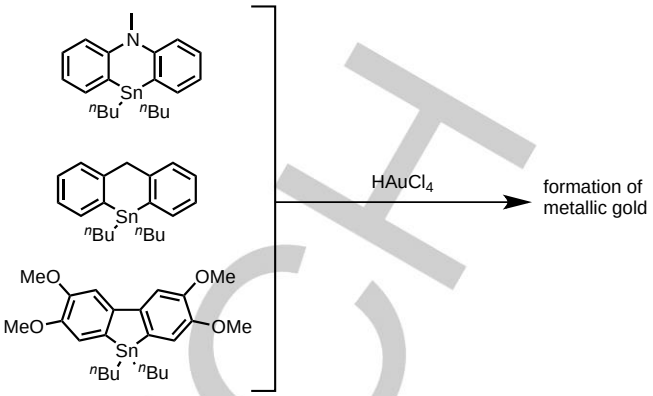

Scheme 2. Attempted transmetallation reactions between modified organostannyl compounds and $HAuCl_4$ salt.

Intermolecular Interactions

The previous report on the cationic [Au(C^N^N)(C≡CC_6H_4-4-NMe_2)]$^+$ complex having an intermolecular Au(III)···Au(III) distance of 3.495 Å in the solid state is one of the few examples exhibiting short contacts between two unsupported Au(III) metal ions.[26] DFT calculations has suggested the presence of weak Au(III)···Au(III) interaction in this complex.[26a] Here, for complexes **7** and **9**, the intermolecular Au(III)···Au(III) separations are 3.408 and 3.453 Å, respectively. It should be noted that two other reports on dimethylgold(III) complexes with β-diketonate also show intermolecular Au(III)···Au(III) distances as short as 3.416 and 3.475 Å.[27]

It was suggested by Pyykkö that Au(III)···Au(III) distances shorter than 3.7 Å could infer the presence of an aurophilic interaction.[28] However, DFT calculations performed on **7** and **9** revealed that these rather short intermolecular distances are due to dispersive interactions between the cyclometalated biphenyl ligand and the acac-ancillary ligand, which accounts for more than 80% of the total dispersion energy (Table 1). This finding is also in accordance with the latest studies on aurophilic attraction by Pyykkö[29] and the non-covalent interactions by Grimme,[18] which both found that the major stabilization energy for non-covalent systems comes from dispersion attraction. Such arrangement is also borne out in the X-ray crystal structures of **7** and **9** which revealed that the two gold ions of the dimer do not lie on the same axis (Figure S45, supporting information); rather, the cyclometalated ligand and ancillary ligands are eclipsed to each other and in a head-to-tail manner, further supporting the notion that ligand-ligand interactions are the dominant factor.

It is also noted that the Au···Au and interplanar distances are longer in the crystal structures of **1** than those of **7** (3.740 and 3.47 Å respectively for **1** and 3.408 and 3.32 Å respectively for **7** Table S9, supporting information). This seems to contradict with the conventional wisdom that the presence of bulky groups in **7** should prevent the close approach of two molecules. It is speculated that the *t*Bu-substituted biphenyl ligand in **7** and **9** have a greater dispersion effect with the acac ligand of another molecule, which outweigh the steric repulsion. Similar observations have been reported by Power and co-workers,[30] e.g., in a distannene molecule, [Sn{SiMetBu$_2$}$_2$]$_2$, the sterically-

This article is protected by copyright. All rights reserved.

Accepted Manuscript

crowded substituents have been shown to stabilize the dimer structure by dispersion forces.[30a]

Photophysical properties of Au^{III}(C^C) complexes

The high emission quantum yields (11–18% in deaerated CH_2Cl_2 and up to 35% in thin-film samples) of complexes **1**–**3**, **7** and **9** may be attributed to the doubly C-deprotonated biphenyl ligand which can effectively destabilize the Au 5dσ* orbital and, hence, the electronic excited states resulting from population of electron into this antibonding dσ* orbital. Inspection of the emission lifetime data reveals that the quenching of emission due to the thermally-accessible deactivating excited state is not significant: the lifetimes of 50–200 μs at room temperature (RT) are only 2 to 4.3 times shorter than those of 120–860 μs measured in 77 K glassy solutions (refer to Table 2). In the literature, the luminescence of many cyclometalated Au(III) complexes is significantly quenched at room temperature. An example is [Au(C^N^C)(C≡CPh)]. Its emission lifetime is significantly reduced from 194 μs at 77 K to less than 0.05 μs at RT. [4c]

The emission of most reported cyclometalated gold(III) complexes comes from ^{3}IL ππ* excited states localized on the cyclometalated ligands, which is usually vibronically-structured with spacings characteristic of C=C/C=N bond stretching. Tuning of emission energy is usually accomplished by modification of the cyclometalated ligand. For example, in the case of [Au(C^N)(C≡CC_6H_4-*p*-OCH_3)$_2$] complexes, by using different [C^N] cyclometalated ligands, the emission energies can be tuned from blue-green (λ_{max} = 464, 492, 524 nm; C^N = phenylpyridine) to red (λ_{max} = 592, 632, 697 nm; C^N = 1-phenylisoquinoline).[5c] In this work, modification of the cyclometalated [C^C] ligand by attaching electron-donating *tert*-butyl substituents could also lead to red-shifts in emission energies; for instance, from **1** to **7**, λ_{max} shifts from 466 to 478 nm. The red shift is presumably caused by a simultaneous destabilization of the π(C^C) and π*(C^C) with the former destabilized to a slightly larger extent.

Complexes **3** and **9** display broad, structureless emission at ca. 585 nm. Photophysical and electrochemical data of **3** and **9**, together with the DFT/TDDFT calculations on **3**, lend support to the lowest-energy emissive excited state being ^{3}ILCT localized on the benzothiophene (bt) β-diketonate ancillary ligand. This assignment is also consistent with an insignificant shift in λ_{max} upon incorporations of the *t*Bu-substituents at the C^C cyclometalated ligand (585 vs 590 nm for complexes **3** and **9** respectively). The relocation of the emissive origin from ^{3}ππ*(C^C) to ^{3}ILCT(O^O) is a consequence of the more extended π-conjugation at the ancillary bt ligand, rendering the energy of the ^{3}ILCT(O^O) excited state lower-lying than the ^{3}ππ*(C^C) excited state.

Similarly, complexes **4a** and **4b** bearing β-diketonate ligands with aryl groups display structureless emission at ca. 500 nm (Figure S27, supporting information) and calculations also suggested that the emission is derived from ^{3}ILCT(O^O) excited states. The emission quantum yields are, however, much smaller than complexes **3** and **9** (Φ_{em} = 16−18 % for **3** and **9** but Φ_{em} <2% for **4a** and **4b**). DFT calculations revealed that there is a significant torsional distortion of the phenyl rings in **4a** when going from the ^{3}ILCT(O^O) excited state to the ground state (e.g., the dihedral angles of the two phenyl rings in the O^O ligand of **4a** change from 14° and 3° at the optimized ^{3}ILCT(O^O) geometry to 27° and −27° at the optimized S_0 geometry, see Figure S48 in the supporting information) while the bt moiety is not free to rotate. Complexes **4a** and **4b** in 77 K glassy solutions show vibronically-structured emissions with energies and profiles similar to that of **1** and could be assigned to ^{3}ππ*(C^C) → S_0 transitions. The fact that there is a switch in the emissive excited state from the lower-lying ^{3}ILCT(O^O) at room temperature to the higher-lying ^{3}ππ*(C^C) at lower temperature (77 K) suggests that the population of the ^{3}ILCT(O^O) excited state comes from energy transfer from the ^{3}ππ*(C^C) with an energy barrier.[31]

It should be noted that in other reported Au(III) complexes, e.g., [Au(C^N^C)L] and [Au(C^N)L_2], the variation in the ancillary ligands (L) generally causes a negligible effect on the emission energy as the emissive excited states are often localized on the cyclometalated ligands, C^N^C and C^N.[4,5] This work demonstrates that, with a judicious choice of the ancillary ligand, it is possible to tune the emission colour by modifications on both the cyclometalated ligands and the ancillary ligands.

Ground state aggregation and excimeric emission

Excimeric emission of transition metal complexes can be useful in white organic light-emitting devices (WOLEDs) because a broad emission spectrum comprised of high-energy monomeric emission and low-energy excimeric emission can be achieved with a single dopant material.[32] It has been recognized that planar molecules favour face-to-face interactions between molecules due to the overlap of orbitals orthogonal to the molecular plane. One of the most representative examples is the d^8 square planar Pt(II) complexes which exhibit favourable Pt(II)···Pt(II) interactions, giving rise to low-energy metal-metal-to-ligand charge transfer (^{3}MMLCT) excimeric emissions in both solutions and the solid state.[11,32] Although Au(III) complexes are also d^8 square planar complexes, excimeric emissions in solutions, solid state or neat film samples have seldom been mentioned in reported Au(III) complexes,[12] as well as the rare observation of Au(III)···Au(III) interactions. Red-shifted emissions due to ground state aggregation of Au(III) complexes,[33] and that self-assembled morphologies of Au(III) complexes driven by hydrophobic interactions or π-π stacking could, nevertheless, be found.[34]

In the present study, an extra *structureless emission* band red-shifted from the monomeric emission band is observed for **1**, **3** and **9** in the solid state at 298 K (λ_{em}: 574, 659 and 683 nm respectively). These spectral features are often exhibited by complexes displaying excimeric emission.[11,35] Time-resolved emission measurements were employed to examine the temporal evolution of the monomeric and low-energy emission bands independently (Figure 11b–d). For the solid sample of **1**, the monomer emission band dominates from 0–15 μs and vanishes completely after 80 μs. On the other hand, a long-lived low-energy emission centred at 574 nm is exclusively observed from 100–1200 μs. Lowering the temperature from 298 K to 77 K results in the disappearance of the low-energy emission band,

This article is protected by copyright. All rights reserved.

suggesting that there is an energy barrier for the formation of the excimer.[36] Similar low-energy emission bands are observed for solid samples of **3** and **9** as well. The key evidence supporting the excimeric emission is same excitation spectra when monitored at all emission maxima, i.e., λ_{em} at 464, 498 and 574 nm (Figure S44, supporting information), suggesting the low-energy emission at 574 nm has originated from the photoexcitation of monomeric species, which only form excimeric species in the excited state.[31a,37] Therefore, we can assign excimeric emissions for **1**, **3** and **9** in the solid state at 298 K. It is however noted that although there are shorter Au-Au and π-π distances in the crystal structures of **7**, but not of **1** **(**Table S9, supporting information), only the latter exhibit excimeric emissions at room temperature in the solid state. Since the solid samples are amorphous, it may suggest that there are less domains with favourable interactions in **7**, indicating the effect of the micro-environments on the photophysics. Another interesting observation is that the decay lifetime for excimeric emission observed in **1** and **3** are much longer than the monomeric emission (more than 50-fold), which is rather atypical in the literature.[11b,38] It is envisaged that the slower non-radiative decay rate of the excimeric emissions and the faster radiative decay of the monomer play a vital role resulting in the abnormal difference in lifetimes between the two.

Conclusions

A new class of strongly luminescent Au(III) complexes, [Au(C^C)(L^X)], supported by the cyclometalated biphenyl ligand and ancillary mono-anionic bidentate ligand is reported. The doubly C-deprotonated biphenyl ligand could destabilize the Au(III) 5dσ* orbital, leading to a reduced excited state structural distortion via electronic population in the Au(III) 5dσ* orbital. Efficient phosphor with Φ_{em} up to 18% in solutions, 35% in thin-film, and a sky-blue OLED device with EQE up to 6.71% have been achieved based on the Au(III) complexes. It is also shown that tuning of the emission energy of Au(III) complexes, apart from the modification on the cyclometalated ligand, can also be achieved by modifying the ancillary ligand, which is seldom reported in the literature. The present work also unveils some rare properties of Au(III) complexes: the observations of excimeric emissions in the solid samples of **1**, **3** and **9**, and the occurrence of short Au(III)···Au(III) intermetal distances in the crystal structures of **7** and **9**, both are reminiscent to the chemistry of luminescent platinum(II) complexes, which is presently a topical area of research in luminescent functional molecular materials.

This work opens up a new entry to the design of luminescent Au(III) complexes, other than the more well-studied [Au(C^N^C)L] or [Au(C^N)L_2] systems, and is envisaged to revive the interests of Au(III) complexes in the supramolecular interactions of d^8 metal complexes.

Experimental Section

Chemical and instrumentation

All chemicals were purchased unless otherwise specified. Reagent grade solvents were used for synthesis. For photophysical measurements and cyclic voltammetric measurements, HPLC grade solvents were used. ^{1}H, ^{13}C, ^{19}F, ^{31}P and ^{11}B nuclear magnetic resonance (NMR) spectra were recorded on a Bruker DPX-300, Avance 400, DRX-500 or Avance 600 NMR spectrometer. Solvents used for NMR measurements were all deuterated. All chemical shifts (δ) were reported in ppm. For all deuterated solvents, the chemical shifts were calibrated with the corresponding solvent residual peaks.[39] The chemical shifts for ^{13}C measured in $CDCl_3$ were calibrated with the ^{13}C signal of $CDCl_3$ at 77.16 ppm. ^{13}C, ^{19}F, ^{31}P and ^{11}B signals are all ^{1}H decoupled. Electron impact (EI) and fast-atom bombardment (FAB) mass spectra were recorded on a Finnigan MAT 95 mass spectrometer. High-resolutin electrospray ionization (HR-ESI) mass spectra were recorded on a Waters Micromass Q-Tof Premier mass spectrometer. Elemental analyses were performed at the Institute of Chemistry, Chinese Acamdemy of Sciences, Beijing, China. Thermogravimetric analyses (TGA) were performed under nitrogen on a Perkin Elmer Pyris1 Thermogravimetric Analyzer; scan rate: 10 °C/min; scan range: 40–800 °C. Transmission electron microscopy (TEM) was performed on a Tecnai G2 20 S-TWIN Scanning Transmission Electron Microscope. Selected-area electron diffraction (SAED) patterns were obtained by subjecting the specimen to parallel beams of high-energy electrons. Cyclic voltmmetric measurements were performed on a Princeton Applied Research electrochemical analyser (Potentiostat/Galvanostat Model 273 A) in a three-compartment cell. Tetrabutylammonium hexafluorophosphate ($^{n}Bu_4NPF_6$, 0.1 M) in CH_2Cl_2, MeCN or DMF was used as the supporting electrolyte throughout this work. The solutions were degassed by argon prior to measurements. $Ag/AgNO_3$ (0.1 M in MeCN), glassy carbon and platinum wire were used as the reference electrode, working electrode and counter electrode, respectively. All measurements were conducted at room temperature. The ferrocenium/ferrocene ($Cp_2Fe^{+/0}$) couple was used as the internal standard.

Photophysical measurements

Ultraviolet-visible light (UV-vis) absorption spectra were recorded on a Hewelett-Packard 8452A Diode Array Spectrophotometer. The spectra were generally obtained with 2×10^{-5} M solutions unless specified. Variable temperature UV-vis absorption spectra was recorded on an Agilent Cary 8454 UV-visiable Spectrscopy System. Steady-state emission and excitation spectra of samples in solutions, solid state or glassy state, were recorded on a SPEX Fluorolog 3 Spectrofluorometer. For measurements in solution at room temperature, samples were placed in a two-compartment cells consisting of a 10 mL-pyrex bulb and a 1-cm path length quartz curvette. The cells were sealed from the atmosphere with Rotaflo stopcocks. Solutions were degassed in a high-vacuum line for five times by freeze-thaw-pump cycles. Luminescence quantum yields (Φ_s) were determined by the method of Demas and Crosby[40] using $[Ru(bpy)_3](PF_6)_2$ in degassed acetonitrile (Φ_r = 0.062) or 9,10-bis(phenylethynyl)anthracence (BPEA) in degassed benzene (Φ_r = 0.85) as the standard. Φ_s values were calculated by the following equation: $\Phi_s=\Phi_r(B_r/B_s)(n_s/n_r)^2(D_s/D_r)$, where the subscripts s and r denote the parameters for sample and reference respectively, n is the refractive index of solvents; D is the integrated emission intensity; $B = 1 - 10^{-AL}$ (where A is the absorbance at the excitation wavelength, L is the optical path length in cm). Solid samples or glassy solutions (EtOH/MeOH = 4:1; concentration: 10^{-6} to 10^{-5} M) were placed in 5-mm quartz tubes. For low-temperature 77 K measurements, the quartz tubes containing the samples were placed in a quartz-walled Dewar filled with liquid nitrogen.

For internal use, please do not delete. Submitted_Manuscript

This article is protected by copyright. All rights reserved.

Emission spectra and absolute emission quantum yields of thin-film samples were recorded on a Hamamatsu Quantaurus-QY Absolute PL quantum yields measurement system C11347. Thin-film samples were prepared by drop-casting chlorobenzene solutions of complex with PMMA or PYD-2Cz (5:95) onto clean quartz-plates. Emission lifetimes (τ) were measured with a Quanta Ray DCR-3 pulsed Nd:YAG laser system (pulse λ_{exc} = 355 nm). Emission decay signals were monitored as a function of time using a R928 photomultiplier tube. The lifetime values were estimated by fitting mono-exponential decay using Origin software. Samples for nanosecond time-resolved emission or nanosecond transient absorption (ns-TA) were prepared in the same way as steady-state photophysical measurements. Measurements were performed on a LP920-KS Laser Flash Photolysis Spectrophotometer (Edinburgh Instruments Ltd). The excitation source was a Q-switched Nd:YAG laser system. Laser excitation wavelength (λ_{ex}) used was 355 nm (the third harmonic line) or 266 nm (the fourth harmonic line). Data were processed with a PC-plugin controlled by the software L900. Femtosecond time-resolved transient absorption (fs-TA) measurements were performed on a HELIOS setup equiped with the Ti:Sapphire regenerative amplifier laser system (Spitfire Pro). Laser λ_{ex} of 400 nm (the second harmonic line) was used. The pump and probe source were the same. The precise delay times were monitored with an optical delay rail. Signals for each measurement were averaged for 1 s.

Crystal structure determination

The X-ray diffraction data were collected on a Bruker X8 Proteum diffractometer. The crystals were kept at 100 K during data collection. The diffraction images were interpreted and the diffraction intensities were integrated by using the program SAINT. By using Olex2,[41] the structure was solved with the ShelXS structure solution program using direct Methods and refined with the XL refinement package using Least Squares minimization.[42] Crystallographic parameters are summarized in Table S1–S2 (Supporting information). CCDC 1528298–1528303 contain the supplementary crystallographic data for this paper. The data can be obtained free of charge from The Cambridge Crystallographic Data Center via www.ccdc.cam.ac.uk/data_request/cif.

Computational details

The hybrid density functional, PBE0,[43] was employed for the calculations on photophysical properties using the program package G09.[16] The 6-31G* basis set[44] is used for all atoms except Au, which is described by the Stuttgart relativistic pseudopotential and its accompanying basis set (ECP60MWB).[45] Solvent effect was also included by means of the polarizable continuum model (PCM)[46] and default parameters are used for the solvent, dichloromethane. No symmetry constraints were applied in geometry optimizations. For the singlet ground state (S_0), the restricted density functional theory (RDFT) formalism was employed. For the triplet excited states ($^3\pi\pi^*$(C^C) and ^{3}ILCT(O^O)) were optimized using both unrestricted DFT (UDFT) and time-dependent density functional theory (TDDFT).[47] Frequency calculations were performed on the optimized structures to ensure that they are minimum energy structures by the absence of imaginary frequency (i.e. NImag = 0). Stability calculations were also performed for all the optimized structures to ensure that all the wavefunctions obtained are stable. Vertical excitation energies of the singlet and triplet excited states were calculated at the optimized ground state geometries based on TDDFT using the linear response approximation (LR-PCM). The absorption spectra were simulated using the program, GaussSum.[48]

Acknowledgements

This work was supported by the Area of Excellence Program (AoE/P-03/08), the National Key Basic Research Program of China (No. 2013CB834802), the Hong Kong Research Grants Council (HKU 17300614) and Basic Research Program of Shenzhen (JCYJ20160229123546997, JCYJ20160530184056-496). This work is also conducted in part using the research computing facilities and/or advisory services offered by Information Technology Services, the University of Hong Kong. Dr. Tsz Lung Lam and Dr. Xiangguo Guan are greatly acknowledged for their helpful discussions.

Keywords: Photophysics • Gold • Noncovalent interactions • Luminescence • Organic light-emitting diodes

[1] a) R. W.-Y. Sun and C.-M. Che, *Coord. Chem. Rev*. **2009**, *253*, 1682-1691; b) C. Gabbiani, A. Casini and L. Messori, *Gold. Bull*. **2007**, *40*, 73-81.

[2] a) Z. Shi and C. He, *J. Org. Chem*. **2004**, *69*, 3669 – 3671; *b*) J. Urbano, A. J. Hormigo, P. de. Frémont, S. P. Nolan, M. M. Díaz-Requejo and P. J. Pérez, *Chem. Commun*. **2008**, 759 – 761.

[3] Some examples of highly-efficient OLED devices fabricated with Au(III) complexes: a) V. K.-M. Au, K. M.-C. Wong, D. P.-K. Tsang, M.-Y. Chan, N. Zhu and V. W.-W. Yam, *J. Am. Chem. Soc.* **2010**, *132*, 14273 – 14278; b) G. Cheng, K. T. Chan, W.-P. To and C.-M. Che, *Adv. Mater*. **2014**, *26*, 2540 – 2546; c) B. Y.-W. Wong, H.-L. Wong, Y.-C. Wong, M.-Y. Chan and V. W.-W. Yam, *Angew. Chem. Int. Ed*. **2017**, *56*, 302 – 305.

[4] a) V. W.-W. Yam, S. W.-K. Choi, T.-F. Lai and W.-K. Lee, *J. Chem. Soc., Dalton Trans.* **1993**, 1001 – 1002; b) C.-W. Chan, W.-T. Wong and C.-M. Che, *Inorg. Chem*. **1994**, *33*, 1266 – 1272; c) V. W.-W. Yam, K. M.-C. Wong, L.-L. Hung and N. Zhu, *Angew. Chem. Int. Ed*. **2005**, *44* 3107 – 3110; d) K. M.-C. Wong, X. Zhu, L.-L Hung, N. Zhu, V. W.-W Yam and H.-S. Kwok, *Chem. Commun*. **2005**, 2906 – 2908; e) K. M.-C. Wong, L.-L. Hung, W. H. Lam, N. Zhu and V. W.-W. Yam, *J. Am. Chem Soc.* **2007**, *129*, 4350 – 4365; f) V. K.-M. Au, K. M.-C. Wong, N. Zhu and V. W.-W. Yam, *J. Am. Chem. Soc*. **2009**, *131*, 9076 – 9085; g) D.-A Roşca, D. A. Smith and M. Bochmann, *Chem. Commun*. **2012**, *48*, 7247 – 7249; h) W.-P. To, G. S.-M. Tong, W. Lu, C. Ma, J. Liu, A. L.-F. Chow and C.-M. Che, *Angew. Chem. Int. Ed*. **2012**, *51*, 2654 – 2657; i) V. K.-M. Au, W. H. Lam, W.-T. Wong and V. W.-W. Yam, *Inorg. Chem*. **2012**, *51*, 7537 – 7545; j) W.-P. To, K. T. Chan, G. S. M. Tong, C. Ma, W.-M. Kwok, X. Guan, K.-H. Low and C.-M. Che, *Angew. Chem. Int. Ed* **2013**, *52*, 6648 – 6652; k) M.-C. Tang, D. P.-K. Tsang, M. M.-Y. Chan, K. M.-C. Wong and V. W.-W. Yam, *Angew. Chem. Int. Ed.* **2013**, *52*, 446 – 449; l) V. K.-M. Au, D. P.-K. Tsang, M.-Y. Chan, N. Zhu and V. W.-W. Yam, *Inorg. Chem.* **2013**, *52*, 12713 – 12725; m) M.-C. Tang, C. K.-M. Chan, D. P.-K. Tsang, Y.-C. Wong, M. M.-Y. Chan, K. M.-C. Wong and V. W.-W. Yam, *Chem. Eur. J*. **2014**, *20*, 15233 – 15241; n) R Kumar, A. Linden and C. Nevado, *Angew. Chem., Int. Ed.*, **2015**, *54*, 14287-14290.

[5] a) J. A. Garg, O. Blacque, T. Fox and K. Venkatesan, *Inorg. Chem*. **2010**, *49*, 11463 – 11472; b) J. A. Garg, O. Blacque and K. Venkatesan, *Inorg. Chem*. **2011**, *50*, 5430 – 5441; c) V. K. M. Au, K. M. C. Wong, N. Zhu and V. W. W. Yam, *Chem. Eur. J*. **2011**, *17*, 130 – 142; *d*) A. Szentkuti, M. Bachmann, J. A. Garg, O. Blacque, and K. Venkatesan, *Chem. Eur. J*. **2014**, *20*, 2585 – 2596; e) A. Szentkuti, J. A. Garg, O. Blacque and K. Venkatesan, *Inorg. Chem*. **2015**, 54, 10748 – 10760; (f) M. Bachmann, J. Terreni, O. Blacque and K. Venkatesan, *Chem. Eur. J*. **2017**, *23*, 3837 – 3849.

Accepted Manuscript

This article is protected by copyright. All rights reserved.

[6] F. A. Cotton, G. Wilkinson, C. A. Murillo and M. Bochmann, *Advanced Inorganic Chemistry*, Wiley and Sons, New York, **1999**.

[7] a) F. F. Hung, W.-P. To, J.-J. Zhang, C. Ma, W.-Y. Wong and C.-M. Che, *Chem. Eur. J*. **2014**, *20*, 8604 – 8614; b) A. R. Browne, N. Deligonul, B. L. Anderson, M. Zeller, A. D. Hunter and T. G. Gray, *Chem. Commun.* **2015**, *51*, 15800 – 15803; c) N. A. Ayoub, A. R. Browne, B. L. Anderson and T. G. Gray, *Dalton Trans.* **2016**, *45*, 3820 – 3830; d) L. Nilakantan, D. R. McMillin and P. R. Sharp, *Organometallics* **2016**, *35*, 2339 – 2347.

[8] K. Li, G. S. M. Tong, Q. W, G. Cheng, W.-Y. Tong, W.-H. Ang, W.-L. Kwong and C.-M. Che, *Chem. Sci*. **2016**, *7*, 1653 – 1673.

[9] a) C. Adachi, M. A. Baldo, M. E. Thompson and S. R. Forrest, *J. Appl. Phys.* **2001**, *90*, 5048 – 5051; b) S. Lamansky, P. Djurovich, D. Murphy, F. Abdel-Razzaq, H.-E. Lee, C. Adachi, P. E. Burrows, S. R. Forrest and M. E. Thompson, *J. Am. Chem. Soc*. **2001**, *123*, 4304 – 4312; *c*) H. Xu, R. Chen, Q. Sun, W. Lai, Q. Su, W. Huang and X. Liu, *Chem. Soc. Rev*. **2014**, *43*, 3259 – 3302.

[10] J. Brooks, Y. Babayan, S. Lamansky, P. I. Djurovich, I.Tsyba, R. Bau and M. E. Thompson, *Inorg. Chem*. **2002**, *41*, 3055 – 3066; *b*) J. A. G. Williams, S. Develay, D. L. Rochester and L. Murphy, *Coord. Chem. Rev.* **2008**, *252*, 2596 – 2611; *c*) Y. Chi and P. T. Chou, *Chem. Soc. Rev.* **2010**, *39*, 638 – 655.

[11] a) J. A. Bailey, M. G. Hill, R. E. Marsh, V. M. Miskowski, W. P. Schaefer and H. B. Gray, *Inorg. Chem.* **1995**, *34*, 4591 – 4599; b) S.-W. Lai, M. C.-W. Chan, K.-K. Cheung and C.-M. Che, *Organometallics* **1999**, *18*, 3327 – 3336; c) S.-W. Lai, M. C.-W. Chan, K.-K. Cheung and C.-M. Che, *Inorg. Chem.* **1999**, *38*, 4262 – 4267.

[12] Recent article on cyclometalated Au(III) complexes displaying excimeric emissions in the solid state: W.-P. To, G. S. M. Tong, C.-W. Cheung, C. Yang, D. Zhou and C.-M. Che, *Inorg. Chem*. **2017**, *56*, 5046 – 5059.

[13] B. David, U. Monkowius, J. Rust, C. W. Lehmann, L. Hyzaka and F. Mohr, *Dalton Trans.* **2014**, *43*, 11059 – 11066.

[14] A. Usón, J. Vicente and M. T. Chicote, *J. Organomet. Chem*. **1980**, *198*, 105 – 112.

[15] M. Joost, L. Estevez, K. Miqueu, A. Amgoune and D. Bourissou, *Angew. Chem. Int. Ed*. **2015**, *54*, 5236 – 5240.

[16] M. J. Frisch; et al. Gaussian 09 (Revision D.01), Gaussian, Inc., Wallingford CT, **2013**.

[17] a) A. D. Becke, *Phys. Rev. A* **1988** *38*, 3098 – 3100; b) C. T. Lee, W. T. Yang, R. G. Parr, *Phys. Rev. B* **1988**, *37*, 785 – 789; c) S. Grimme, J. Antony, S. Ehrlich and H. Krieg, *J. Chem. Phys*. **2010**, *132*, 154104-1 – 154104-19; d) S. Grimme, *J. Comput. Chem*. **2006**, *27*, 1787 – 1799.

[18] S. Grimme and J. P. Djukic, *Inorg. Chem*. **2011**, *50*, 2619 – 2628.

[19] a) C. Yang, S.-L. Lai, S. L.-F. Chan, K.-H. Low, G. Cheng, K.-T. Yeung, C.-C. Kwok and C.-M. Che, *Chem. Asian. J.* **2014**, **9**, 3572 – 3585; b) S. L.-F. Chan, K.-H. Low, C. Yang, S. H.-F. Cheung and C.-M. Che, *Chem. Eur. J.* **2011**, *17*, 4709 – 4714.

[20] a) H. Yersin and D. Donges, J. K. Nagle, R. Sitters and M. Glasbeek, *Inorg. Chem*. **2000**, *39*, 770 – 777; b) N. M. Shavaleev, H. Adams, J. Best, R. Edge, S. Navaratnam and J. A. Weinstein, *Inorg. Chem*. **2006**, *45*, 9410 – 9415.

[21] Selected examples: a) A. M. Prokhorov, T. Hofbeck, R Czerwieniec, A. F. Suleymanova, D. N. Kozhevnikov, and H. Yersin, *J. Am. Chem. Soc*. **2014**, 136, 9637−9642; b) C. Shi, D. Tu, Q. Yu, H. Liang, Y. Liu, Z. Li, H. Yan, Q. Zhao, and W. Huang, *Chem. Eur. J.* **2014**, 20, 16550 – 16557; c) G. K.-M. So, G. Cheng, J. Wang, X. Chang, C.-C. Kwok, H. Zhang, and C.-M. Che, *Chem. Asian J*. **2017**, DOI: 10.1002/asia.201700081.

[22] N. R. Evans, L. S. Devi, C. S. K. Mak, S. E. Watkins, S. I. Pascu, A. Köhler, R. H. Friend, C. K. Williams and A. B. Holmes, *J. Am. Chem. Soc.* **2006**, *128*, 6647 – 6656.

[23] a) Q. Zhang, T. Komino, S. Huang, S. Matsunami, K. Goushi and C. Adachi, *Adv. Funct. Mater.* **2012**, *22*, 2327 – 2336; b) C. Han, Y. Zhao, H. Xu, J. Chen, Z. Deng, D. Ma, Q. Li and P. Yan, *Chem. Eur. J.* **2011**, *17*, 5800 – 5803; c) F.-M. Hsu, C.-H. Chien, C.-F. Shu, C.-H. Lai, C.-C. Hsieh, K.-W. Wang and P.-T. Chou, *Adv. Funct. Mater*. **2009**, *19*, 2834 – 2843.

[24] A. Steffen, R. M. Ward, W. D. Jones and T. B. Marder, *Coord. Chem. Rev.* 2010, **254**, 1950.

[25] C.-Y. Wu, T. Horibe, C. B. Jacobsen and F. D. Toste, *Nature* **2015**, *517*, 449 – 454.

[26] a) W. Lu, K. T. Chan, S.-X. Wu, Y. Chen and C.-M. Che, *Chem. Sci.* **2012**, *3*, 752 – 755; b) O. Crespo, M. C. Gimeno, A. Laguna, S. M.-Pérez and M. D. Villacampa, *Organometallics* **2012**, *31*, 5520 – 5526; c) V. K.-M. Au, D. P.-K. Tsang, Y.-C. Wong, M.-Y. Chan and V. W.-W. Yam, *J. Organomet. Chem*. **2015**, *792*, 109 – 116.

[27] a) G. I. Zharkova, I. A. Baidina and I. K. Igumenov, *J. Struct. Chem.* **2007**, *48*, 906 – 913; (b) G. I. Zharkova, I. A. Baidina and I. K. Igumenov, *J. Struct. Chem.* **2006**, *47*, 1117 – 1126.

[28] F. Mendizabal and P. Pyykkö, *Phys. Chem. Chem. Phys.* **2004**, *6*, 900 – 905.

[29] J. Muniz, C. Wang and P. Pyykkö, *Chem. Eur. J*. **2011**, *17*, 368 – 377.

[30] a) J.-D. Guo, D. J. Liptrot, S. Nagase and P. P. Power, *Chem. Sci*. **2015**, *6*, 6235 – 6244; b) C.-Y. Lin, J.-D. Guo, J. C. Fettinger, S. Nagase, F. Grandjean, G. J. Long, N. F. Chilton and P. P. Power, *Inorg. Chem*. **2013**, *52*, 13584 – 13593.

[31] E. J. McLaurin, L. R. Bradshaw and D. R. Gamelin, *Chem. Mater*. **2013**, *25*, 1283 – 1292.

[32] a) B. D'Andrade, J. Brooks, V. Adamovich, M. E. Thompson and S. R. Forrest, *Adv. Mater.* **2002**, *12*, 1032 – 1036; b) V. Adamovich, J. Brooks A. Tamayo, A. M. Alexander, P. I. Djurovich, B. W. D'Andrade, C. Adachi, S. R. Forrest and M. E. Thompson, *New. J. Chem*. **2002**, *26*, 1171 – 1178; c) B. D'Andrade and S. R. Forrest, *Chem. Phys*. **2003**, *286*, 321 – 335; d) M. Cocchi, J. Kalinowski, L. Murphy, J. A. G. Williams and V. Fattori, *Org. Electron*. **2010**, *11*, 388 – 396; e) T. Fleetham, J. Ecton, Z. Wang, N. Bakken and J. Li, *Adv. Mater*. **2013**, *25* 2573 – 2576; f) G. Cheng, S. C. F. Kui, W.-H. Ang, M.-Y. Ko, P.-K. Chow, C.-L. Kwong, C.-C. Kwok, C. Ma, X. Guan, K.-H. Low, S.-J. Su and C.-M. Che, *Chem Sci*. **2014**, *5*, 4819 – 4830.

[33] L. Currie, J. Fernandez-Cestau, L. Rocchigiani, B. Bertrand, S. J. Lancaster, D. L. Hughes, H. Duckworth, S. T. E. Jones, D. Credgington, T. J. Penfold and M. Bochmann, *Chem. Eur. J*. **2017**, *23*, 105 – 113.

[34] a) J. J. Zhang, W. Lu, R. W. Y. Sun and C.-M. Che, *Angew. Chem. Int. Ed*. **2012**, *51*, 4882 – 4886; b) V. K.-M. Au, N. Zhu and V. W.-W. Yam, *Inorg. Chem*. **2013**, *52*, 558 – 567; c) K.-C. Yim, E. S.-H. Lam, K. M.-C. Wong, V. K.-M. Au, C.-C. Ko, W. H. Lam and V. W.-W. Yam, *Chem. Eur. J*. **2014**, *20*, 9930 – 9939; d) K.-C. Yim, V. K.-M. Au, L.-L. Hung, K. M.-C. Wong and V. W.-W. Yam, *Chem. Eur. J*. **2016**, *22*, 16258 – 16270.

[35] a) B. Valeur, *Molecular Fluorescence – Principles and Applications*; Wiley-VCH Verlag GmbH; Weinheim, **2002**; b) B. Ma, P. I. Djurovich and M. E. Thompson, *Coord. Chem. Rev.* **2005**, *249*, 1501 – 1510.

[36] T. Ogawa, M. Yoshida, H. Ohara, A. Kobayashi and M. Kato, *Chem. Commun*. **2015**, *51*, 13377 – 13380.

[37] J. Kalinowski, M. Cocchi, L. Murphy, J. A. G. Williams and V. Fattori, *Chem. Phys*. **2010**, *378*, 47 – 57.

[38] The monomeric and excimeric emission lifetimes of Pt(4,4'-di-*tert*butylbipyridine)$(CN)_2$] in 1,2-dichloroethane solutions at RT are 2.9 µs and 40 ns respectively: K.-T. Wan, C.-M. Che and K. C. Cho, *J. Chem. Soc. Dalton Trans.* **1991**, 1077 – 1080.

[39] G. R. Fulmer, A. J. M. Miller, N. H. Sherden, H. E. Gottlieb, A. Nudelman, B. M. Stoltz, J. E. Bercaw and K. I. Goldberg, *Organometallics* **2010**, *29*, 2176 – 2179.

[40] J. N. Demas and G. A. Crosby, *J. Phys. Chem*. **1971**, *75*, 991 – 1024.

[41] O. V. Dolomanov, L. J. Bourhis, R. J. Gildea, J. A. K. Howard and H. Puschmann, *J. Appl. Cryst.* **2009**, *42*, 339 – 341.

[42] G. Sheldrick, *Acta Cryst. A* **2008**, *64*, 112 – 122.

[43] C. Adamo and V. Barone, *J. Chem. Phys.* **1999**, *110*, 6158–6170.

Accepted Manuscript

This article is protected by copyright. All rights reserved.

[44] a) M. M. Francl, W. J. Petro, W. J. Hehre, J. S. Binkley, M. S. Gordon, D. J. DeFree and J. A. Pople, *J. Chem. Phys.* **1982**, *77*, 3654–3665; b) P. C. Hariharan and J. A. Pople, *Theor. Chim. Acta* **1973**, *28*, 213–222.

[45] a) D. Andrae, U. Haeussermann, M. Dolg, H. Stoll and H. Preuss, *Theor. Chim. Acta* **1990**, *77*, 123–141; b) J. M. L. Martin and A. Sundermann, *J. Chem. Phys.* **2001**, *114*, 3408 – 3420.

[46] M. Cossi, G. Scalmani, N. Rega and V. Barone, *J. Chem. Phys.* **2002**, *117*, 43 – 54.

[47] G. Scalmani, M. J. Frisch, B. Mennucci, J. Tomasi, R. Cammi and V. Barone, *J. Chem. Phys.* **2006**, *124*, 094107-1 – 094107-15.

[48] N. M. O'Boyle, A. L. Tenderholt and K. M. Langner, *J. Comp. Chem.* **2008**, *29*, 839 – 845.

WILEY-VCH

Accepted Manuscript

This article is protected by copyright. All rights reserved.

Entry for the Table of Contents (Please choose one layout)

Layout 1:

FULL PAPER

Strongly luminescent cyclometalated Au(III) complexes supported by bidentate ligands exhibit emission quantum yields up to 18% in solutions, 35% in thin-films, tunable emission energy, short intermetal distances and excimeric emission in the solid state.

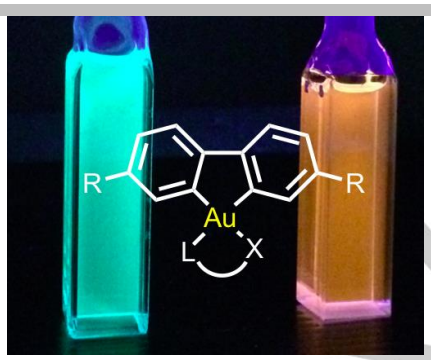

*Author(s), Corresponding Author(s)**

Page No. – Page No.

Title

Layout 2:

FULL PAPER

((Insert TOC Graphic here; max. width: 11.5 cm; max. height: 2.5 cm))

*Author(s), Corresponding Author(s)**

Page No. – Page No.

Title

Text for Table of Contents

This article is protected by copyright. All rights reserved.

WILEY-VCH Accepted Manuscript